

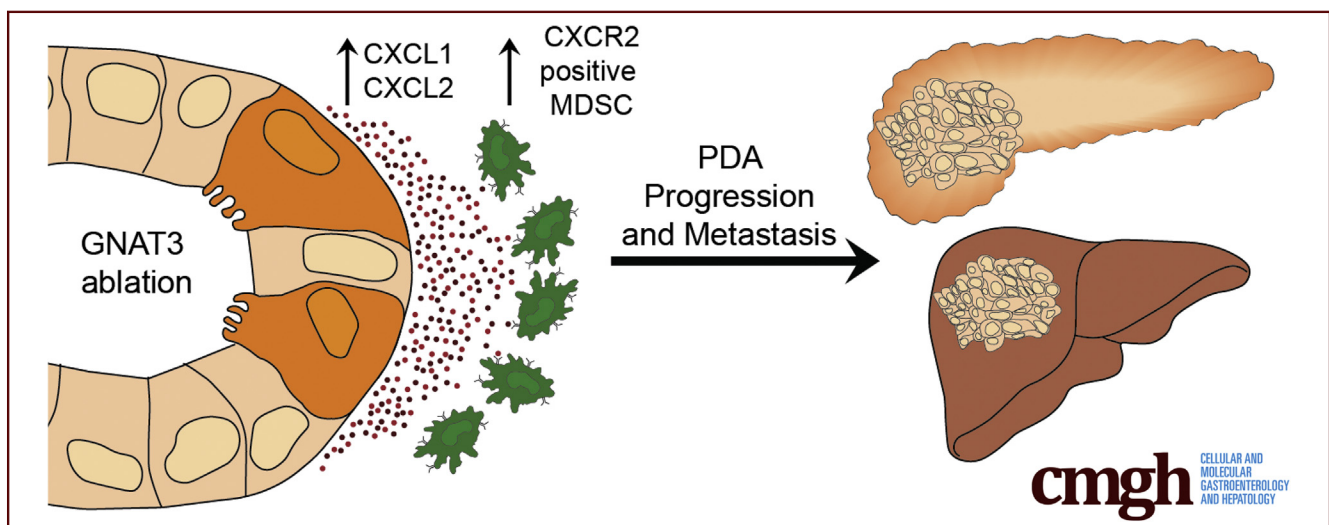
ORIGINAL RESEARCH

The Gustatory Sensory G-Protein GNAT3 Suppresses Pancreatic Cancer Progression in Mice



Megan T. Hoffman,^{1,2} Samantha B. Kemp,^{1,3} Daniel J. Salas-Escabillas,^{1,2} Yaqing Zhang,^{1,4} Nina G. Steele,^{1,4,5} Stephanie The,⁶ Daniel Long,^{1,2} Simone Benitz,^{1,2} Wei Yan,^{1,4} Robert F. Margolskee,⁷ Filip Bednar,^{1,4} Marina Pasca di Magliano,^{1,4,5} Hui-Ju Wen,^{1,2} and Howard C. Crawford^{1,2}

¹Rogel Comprehensive Cancer Center, ²Department of Molecular and Integrative Physiology, ³Department of Pathology, ⁴Department of Surgery, ⁵Department of Cell and Developmental Biology, and ⁶Department of Computational Medicine and Bioinformatics, University of Michigan, Ann Arbor, Michigan; and ⁷Monell Chemical Senses Center, Philadelphia, Pennsylvania



SUMMARY

GNAT3 ablation enhances CXCL1 and CXCL2 epithelial expression and increases the number of CXCR2 expressing myeloid-derived suppressor cells with altered immunomodulatory gene expression. Analysis of long-term ablation during pancreatic cancer progression found increased metastatic carcinoma.

BACKGROUND & AIMS: Pancreatic ductal adenocarcinoma (PDA) initiation and progression are accompanied by an immunosuppressive inflammatory response. Here, we evaluated the immunomodulatory role of chemosensory signaling in metaplastic tuft cells (MTCs) by analyzing the role of GNAT3, a gustatory pathway G-protein expressed by MTCs, during PDA progression.

METHODS: *Gnat3*-null (*Gnat3*^{-/-}) mice were crossbred with animals harboring a Cre-inducible *Kras*^{LSL-G12D/+} allele with either *Ptf1a*^{Cre/+} (KC) or tamoxifen-inducible *Ptf1a*^{CreERT/+} (KC^{ERT}) mice to drive oncogenic KRAS expression in the pancreas. Ex vivo organoid conditioned medium generated from KC and *Gnat3*^{-/-};KC acinar cells was analyzed for cytokine secretion. Experimental pancreatitis was induced in KC^{ERT} and *Gnat3*^{-/-};KC^{ERT} mice to accelerate tumorigenesis, followed by analysis using mass

cytometry and single-cell RNA sequencing. To study PDA progression, KC and *Gnat3*^{-/-};KC mice were aged to morbidity or 52 weeks.

RESULTS: Ablation of *Gnat3* in KC organoids increased release of tumor-promoting cytokines in conditioned media, including CXCL1 and CXCL2. Analysis of *Gnat3*^{-/-};KC^{ERT} pancreata found altered expression of immunomodulatory genes in *Cxcr2* expressing myeloid-derived suppressor cells (MDSCs) and an increased number of granulocytic MDSCs, a subset of tumor promoting MDSCs. Importantly, expression levels of CXCL1 and CXCL2, known ligands for CXCR2, were also elevated in *Gnat3*^{-/-};KC^{ERT} pancreata. Consistent with the tumor-promoting role of MDSCs, aged *Gnat3*^{-/-};KC mice progressed more rapidly to metastatic carcinoma compared with KC controls.

CONCLUSIONS: Compromised gustatory sensing, achieved by *Gnat3* ablation, enhanced the CXCL1/2–CXCR2 axis to alter the MDSC population and promoted the progression of metastatic PDA. (*Cell Mol Gastroenterol Hepatol* 2021;11:349–369; <https://doi.org/10.1016/j.jcmgh.2020.08.011>)

Keywords: Tuft Cell; MDSC; CXCL1; CXCL2.

Pancreatic ductal adenocarcinoma (PDA) is predicted to become the second leading cause of cancer death by 2030 if no progress is made to improve its current 10% 5-year survival rate.^{1,2} Because of nonspecific symptoms, most patients are diagnosed at a late stage when treatments, including surgery and chemotherapy, are minimally effective.^{3,4} The discovery of novel markers for early stage detection is likely to be guided by understanding alterations in the pancreas during PDA tumorigenesis.

An early step in pancreatic transformation is a process called acinar-to-ductal metaplasia (ADM), which can also be induced by pancreatic injury.^{5,6} ADM formation and the development of early pancreatic intraepithelial neoplasia (PanIN) are driven by oncogenic KRAS mutations,^{7,8} which are found in >90% of PDAs.^{9,10} Additional mutations in tumor suppressor genes such as *CDKN2A*, *TRP53*, and *SMAD4* drive neoplastic progression and eventually PDA.^{11,12} Accompanying ADM is a coordinated immune influx that can modify or sustain ADM and promote PanIN formation and progression.¹³ This immune response is highly immunosuppressive, allowing immune evasion and promoting tumor growth.¹⁴ Multiple immune populations contribute to this immunosuppressive microenvironment, with the myeloid lineage, in particular, playing a critical role in this process.¹⁴ Two major types of myeloid cells, tumor-associated macrophages (TAMs) and myeloid-derived suppressor cells (MDSCs), promote immune evasion by reducing the influx and function of cytotoxic T cells through multiple mechanisms including expression of immune checkpoint ligands.¹⁴ Both TAMs and MDSCs are present in early and late stages of pancreatic lesions and create a barrier for treatment of PDA by immune targeted or chemotherapeutic treatments.^{14,15}

ADM and PanIN lesions are composed of a heterogeneous population of cell subtypes,^{16–18} with 1 unique cell type identified in these lesions as the metaplastic tuft cell (MTC).¹⁹ Normal tuft cells are solitary chemosensory cells associated with sensing and responding to stimuli within the luminal spaces of many hollow organs throughout the body, including the bile duct and intestine.²⁰ In the intestine and nasal cavity, normal tuft cells can detect pathogens and subsequently signal to nearby cells to mount an immune response.^{21–23} These sensory and immunomodulatory functions of tuft cells require functional gustatory signaling machinery, including transient receptor potential cation channel subfamily M member 5 (TRPM5), α -gustducin (GNAT3), and G-protein coupled taste receptors, all components of the canonical taste sensory pathway.^{20,24} The detection of sensory cues through the canonical gustatory pathway stimulates apical taste receptors activating GNAT3-dependent calcium efflux and subsequent activation of TRPM5 cation channels.²⁵ Plasma membrane depolarization, driven by cation influx, promotes release of signaling molecules from intracellular stores to activate external cell responses, including nerve cell communication and immune cell activation.^{24,25} In the normal mouse pancreas, tuft cells are only found in the common bile duct that passes through the head of the organ.¹⁹ However, MTCs are a

prominent cell type in ADM and PanINs and express TRPM5, GNAT3, and immunomodulatory molecules, suggesting they are fully functional and may influence the immune system during PDA progression.¹⁹

In our current study, we compromised the chemosensory function of MTCs by ablating *Gnat3* in complementary models of pancreatic transformation. Surprisingly, *Gnat3* ablation increased the levels of different chemokines, including CXCL1 and CXCL2, in an ex vivo 3-dimensional organoid culture model. In vivo, GNAT3 loss in a KRAS-driven model of pancreatic neoplasia had no impact on initial transformation but showed increased infiltrating granulocytic MDSCs (gMDSCs), a subtype of tumor promoting MDSCs.¹⁷ In addition, single-cell RNA sequencing revealed an enhanced immunosuppressive gene signature in the MDSC population. Increased CXCL1 and CXCL2 were found in the GNAT3 ablated neoplastic lesions, whereas CXCR2, their cognate receptor, was found primarily expressed in MDSCs. The CXCL1/2-CXCR2 axis is known to promote PDA by altering MDSC and neutrophil recruitment and function.^{26,27} Consistent with this, pancreatic neoplasia progressed more rapidly to metastatic cancer in *Gnat3* ablated mice.


Results

Gnat3 Ablation in *Kras*^{G12D}-Expressing Epithelial Cells Increases CXCL1 and CXCL2 Levels

Normal tuft cell chemosensory signaling drives alteration of the immune microenvironment during parasitic and bacterial infection,^{21–23} leading us to hypothesize that MTCs play a similar immune modulatory role during PDA progression. Alpha-gustducin (encoded by the gene *Gnat3*) is a G protein critical for a gustatory response to bitter, sweet, and umami stimuli in the taste bud but is also critical for normal tuft cell function.^{21,28} To test the contribution of MTC chemosensory function to pancreatic tumor progression, we used a *Gnat3* knockout (*Gnat3*^{-/-}) mouse to compromise MTC chemosensation in mouse models of pancreatic neoplasia.²⁹

Pancreata of *Gnat3*^{-/-} mice showed no difference in pancreas histology and pancreas-to-body weight ratios compared with wild-type (WT) controls (Figure 1A).

Abbreviations used in this paper: ADM, acinar-to-ductal metaplasia; BSA, bovine serum albumin; CC3, cleaved caspase 3; CK19, cytokeratin 19; DCLK1, doublecortin-like kinase 1; ELISA, enzyme-linked immunosorbent assay; FBS, fetal bovine serum; gMDSC, granulocytic myeloid-derived suppressor cell; GNAT3, α -gustducin; HBSS, Hank's balanced salt solution; IHC, immunohistochemistry; KC, *Kras*^{G12D/+}; *Ptf1a*^{Cre/+}, KC^{ERT}; *Kras*^{G12D/+}, *Ptf1a*^{CreERT/+}; MDSC, myeloid-derived suppressor cell; mMDSC, monocytic myeloid-derived suppressor cell; MTC, metaplastic tuft cell; NK, natural killer; PanIN, pancreatic intraepithelial neoplasia; PBS, phosphate-buffered saline; PDA, pancreatic ductal adenocarcinoma; PTOM, pancreatic progenitor and tumor organoid media; TAM, tumor-associated macrophage; TRPM5, transient receptor potential cation channel subfamily M member 5; UMAP, Uniform Manifold Approximation and Projection; WT, wild-type.

 Most current article

© 2020 The Authors. Published by Elsevier Inc. on behalf of the AGA Institute. This is an open access article under the CC BY-NC-ND license (<http://creativecommons.org/licenses/by-nc-nd/4.0/>).

2352-345X

<https://doi.org/10.1016/j.jcmgh.2020.08.011>

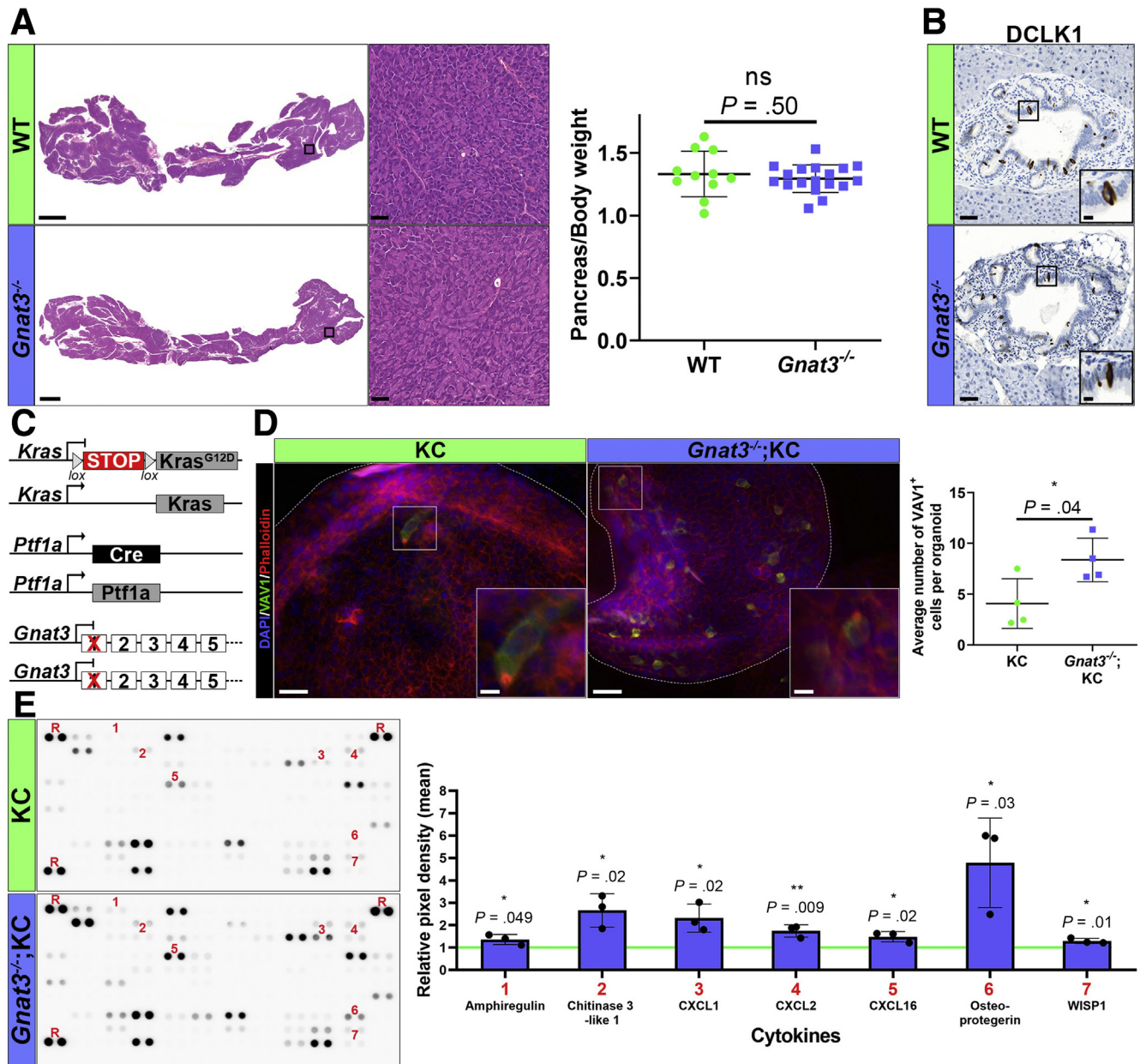


Figure 1. *Gnat3* ablation increases epithelial cytokine release in ex vivo organoid culture model. (A) Analysis of WT or *Gnat3*^{-/-} adult pancreata by H&E, including *magnified inset* from box, and pancreas to body weight ratios (n = 11; 18). Scale bar: 2000 μ m, inset = 50 μ m. (B) IHC for DCLK1 to mark MTCs on WT or *Gnat3*^{-/-} common biliary ducts. Magnified inset indicated in *black box* in bottom right. Scale bar: 50 μ m, inset = 10 μ m. (C) Genetic strategy to generate KC mice with *Gnat3* ablation (*Gnat3*^{-/-};KC). (D) 3D organoid culture analysis of KC and *Gnat3*^{-/-};KC transdifferentiated acinar cells. Phalloidin (*red*) highlights the structure of individual 3D organoids (*white dotted outline*) stained for VAV1 (*green*) to mark MTCs and DAPI (*blue*) to mark nuclei. *White box* denotes inset image in bottom right of VAV1-positive MTCs with tufts marked by phalloidin. MTC numbers were determined from average of 130 organoids per sample (n = 4). Scale bar: 20 μ m, inset = 5 μ m. (E) Cytokine proteomic analysis of conditioned media derived from KC and *Gnat3*^{-/-};KC organoids. Representative cytokine array blot (*left*) and quantitation (*right*) show 7 differentially expressed proteins (numbered). Differential protein levels from *Gnat3*^{-/-};KC (*blue bars*) were normalized by KC (*green line*) (n = 3). R, reference points; 1, amphiregulin; 2, chitinase 2-like 1; 3, CXCL1; 4, CXCL2; 5, CXCL16; 6, osteoprotegerin; 7, WISP1. Significance was calculated using an unpaired *t* test; *P* < .05 statistically significant.

Furthermore, normal tuft cell presence in the common bile duct was not different in *Gnat3*^{-/-} and WT animals, as assessed by immunohistochemistry (IHC) (staining for double cortin-like kinase 1 [DCLK1]) (Figure 1B). Previous work in our lab has found that GNAT3-expressing MTCs

form within ADM and PanIN lesions in the *Kras*^{LSL-G12D/+}; *Ptf1a*^{Cre/+} (KC) model.¹⁹ Therefore, to study the role of *Gnat3* in MTCs in pancreatic neoplasia, we used the KC model crossed with *Gnat3*^{-/-} mice to create the *Gnat3*^{-/-};KC model (Figure 1C).

Primary acinar cell explants were isolated from 8- to 10-week old KC and *Gnat3*^{-/-};KC mice, when the pancreas is still largely devoid of metaplasia and neoplasia, and cultured on a layer of Matrigel in pancreatic progenitor and tumor organoid medium (PTOM), which is sufficient to drive ADM.^{30,31} As expected, acinar cells underwent ADM within 2 days and could be propagated for several months. MTCs were stained in organoids and were found after 7 days of culture and persisted throughout culture duration. In *Gnat3*^{-/-};KC cultures we consistently found higher numbers of MTCs, as quantitated by Vav1 guanine nucleotide exchange factor staining,³⁰ suggesting possible compensatory tuft cell genesis when their sensory function is impaired (Figure 1D). To assay differential signaling from the epithelial compartment, cytokine arrays were performed on 3 biological replicates of KC and *Gnat3*^{-/-};KC organoid conditioned media post-MTC generation (Figure 1E). Expecting that loss of the ability to respond to stimuli would lead to a reduction in cytokine release,²³ we were surprised to find that *Gnat3*^{-/-};KC media instead showed a consistent increase in 7 cytokines (Figure 1E). Interestingly, many of these cytokines, including amphiregulin,^{32,33} chitinase 3-like 1,³⁴ CXCL1,^{17,27,35} CXCL2,²⁶ CXCL16,^{36,37} and osteopontin³⁸ are associated with promoting PDA progression and decreased survival. These data suggest that altering the ability of MTCs to respond to environmental cues leads to dysregulated release of trophic signals and cytokines that will promote PDA progression.

Gnat3 Ablation Does Not Affect Early Pancreatic Neoplastic Progression

To explore how loss of MTC chemosensory function affects pancreatic tumor development, we crossed *Gnat3*^{-/-} mice into the inducible *Kras*^{LSL-G12D/+}; *Ptf1a*^{CreERT/+} (KC^{ERT}) model of pancreatic neoplasia. This model allows for the well-controlled acinar cell-specific expression of oncogenic KRAS after tamoxifen treatment in the adult animal³⁹ (Figure 2A). To accelerate transformation, we then induced acute pancreatitis with supramaximal doses of cerulein, as previously described⁸ (Figure 2A). To determine the optimal time point to study the role of MTCs during disease progression, pancreata were harvested 1 week and 6 weeks after cerulein treatment (Figure 2B). Although ADM lesions were present at both time points, we found few MTCs after 1 week of recovery but a large number after 6 weeks of recovery (Figure 2B). Similar to our acinar explants, these data suggest that generation of MTCs does not coincide with ADM itself but requires additional time (Figure 2B). Therefore, the 6-week time point was chosen for further analysis, because MTCs were present in the context of widespread transformation. We also characterized known MTC marker expression¹⁹ and found no differences in *Gnat3*^{-/-};KC^{ERT} MTCs, with the exception of GNAT3 itself (Figure 2C).

Data from our organoid cultures suggested that GNAT3 loss promotes the release of pro-tumor cytokines. However, despite *Gnat3* ablation, we found no apparent differences in early stage pancreatic neoplasia by

histology, pancreas-to-body weight ratios (a measure of neoplastic burden), or amylase and cytokeratin 19 (CK19) staining, measures of acinar cell dropout and ADM/PanIN genesis, respectively (Figure 3A). We found no difference in collagen deposition assessed by picrosirius red stain (Figure 3B, left). We also found no difference in proliferation by Ki67 staining but did observe an overall increase in epithelial cell apoptosis, measured by cleaved caspase 3 (CC3) IHC, indicating a difference in epithelial cell turnover (Figure 3B, middle). We also found an increase in MTC number, marked by DCLK1 staining, in the neoplastic lesions, similar to the ex vivo 3-dimensional culture model (Figure 3B, right). Overall, we conclude that *Gnat3* loss does not cause any profound changes in early KRAS-induced pancreatic transformation. This may be expected from the delayed MTC genesis compared with ADM formation. However, MTC hypertrophy and increased epithelial cell turnover suggest subtle alterations that may have significant consequences later in progression.

Myeloid-Derived Suppressor Cells Are Increased in Gnat3 Ablated Mice During Pancreatic Transformation

The immune system plays a critical role in initiation and progression of pancreatic disease.⁴⁰ Results from our cytokine array indicate that loss of *Gnat3* increases the release of cytokines, potentially affecting immune cell recruitment during pancreatic transformation. To examine this possibility, KC^{ERT} and *Gnat3*^{-/-};KC^{ERT} tissues were analyzed by mass cytometry to assay 16 different stromal and immune cell markers simultaneously, optimizing for characterization of immune cell populations.⁴¹ We found no difference in the number of fibroblasts or overall immune cells between KC^{ERT} and *Gnat3*^{-/-};KC^{ERT} samples (Figure 4A). We also found no difference in B cells, total T cells, or CD4⁺/CD8⁺ T-cell populations (Figure 4B and C). Macrophages, expressing both proinflammatory and anti-inflammatory polarity markers,^{42,43} were labeled TAMs and were also unchanged (Figure 4D). In a previous study, compromising tuft cell function led to a decrease of natural killer (NK) T cells,⁴⁴ but we found no difference in the NK T-cell (NK1.1⁺CD3⁺) population between tissues (Figure 4E). NK cells, marked by NK1.1⁺CD3⁺, trended lower in *Gnat3*^{-/-};KC^{ERT} pancreata, but this difference did not reach statistical significance (Figure 4E). Likewise, overall numbers of non-TAM myeloid cells, including dendritic cells and MDSCs, were not different than control in the *Gnat3* ablated neoplastic pancreas. However, there were significantly greater numbers of gMDSCs, a subset of MDSCs that are known to contribute to an immunosuppressive tumor microenvironment and promote PDA progression (Figure 4F).⁴⁵⁻⁴⁷

Gnat3 Ablation Alters MDSC Gene Expression in Early Neoplasia

Finding few differences in immune cell numbers, we then analyzed gene expression within the immune population by using single-cell RNA sequencing on KC^{ERT} and

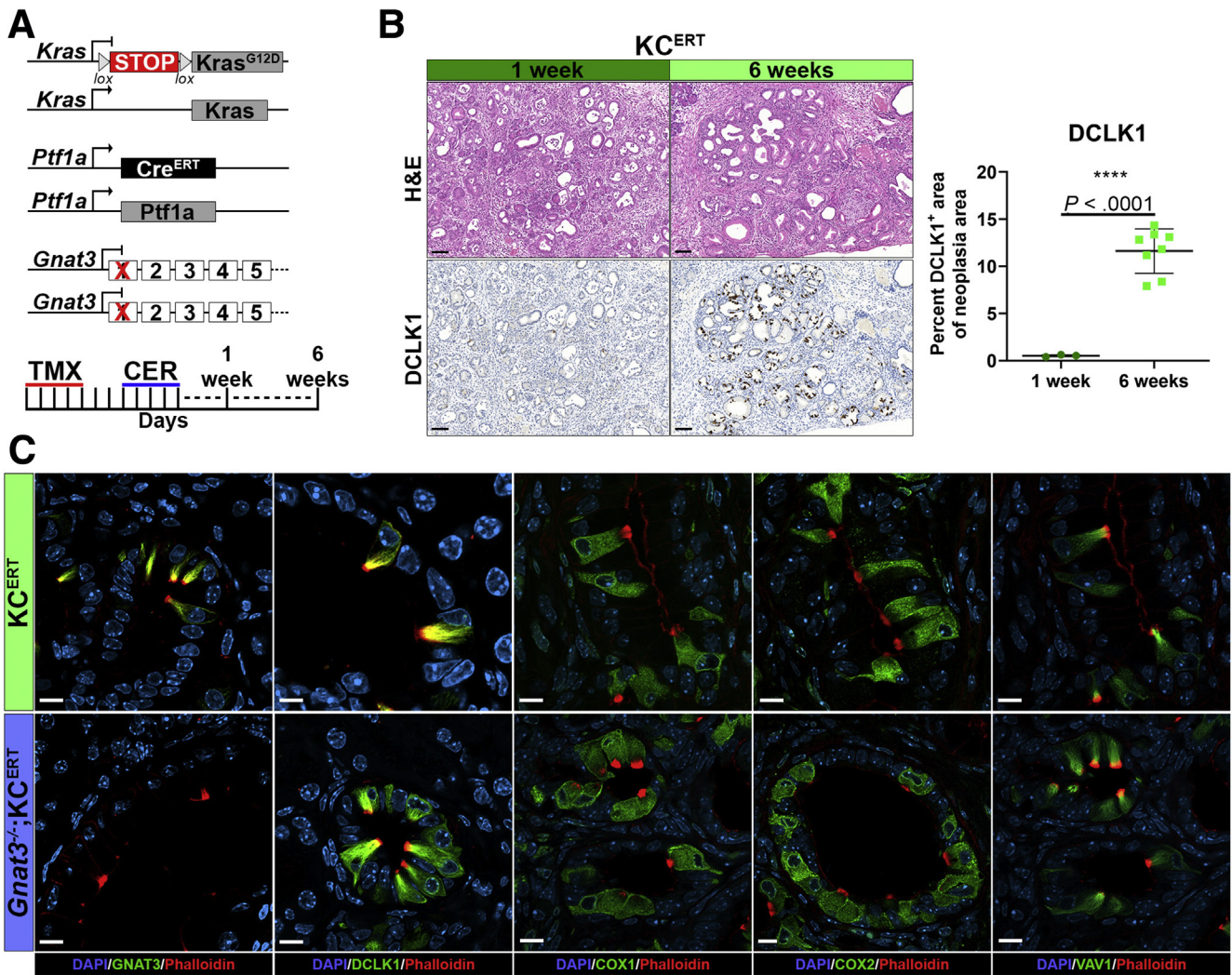


Figure 2. Metaplastic tuft cells are present 6 weeks after injury, and *Gnat3* ablated cells maintain tuft marker expression. (A) Genetic strategy to generate KC^{ERT} mice with *Gnat3* ablation (*Gnat3*^{-/-};KC^{ERT}). Schematic of tamoxifen (TMX) treatment to induce *Kras*^{G12D/+} expression in the acinar compartment, followed by cerulein (CER) to promote inflammation and harvest of pancreas at 1 or 6 weeks. (B) H&E and IHC for DCLK1 to mark MTCs from pancreata harvested from KC^{ERT} mice 1 or 6 weeks after cerulein. Quantitation of DCLK1-positive MTCs from neoplastic area in 1- or 6-week tissue (n = 3; 8). Scale bar: 100 μ m. (C) Staining from 6-week post injury KC^{ERT} and *Gnat3*^{-/-};KC^{ERT} pancreatic tissues for known MTC markers: GNAT3, DCLK1, COX1, COX2, and VAV1 (all green), counterstained by phalloidin (red) to mark the luminal tufts and DAPI (blue) to label nuclei. Scale bars: 5 μ m. Significance was calculated using an unpaired *t* test; $P < .05$ statistically significant.

Gnat3^{-/-};KC^{ERT} mice 6 weeks after cerulein treatment. We optimized tissue processing for recovering and profiling of the immune cell populations, leaving few epithelial cells and fibroblasts in the analysis. Using unsupervised clustering and Uniform Manifold Approximation and Projection (UMAP) visualization,⁴⁸ we identified many distinct cell populations, including multiple T-cell subsets (CD4⁺ T cells, CD8⁺ T cells, and T-regulatory cells) and fibroblast subsets (iCAF and myCAF), which have been previously identified in PDA^{16,49} (Figure 5A and B). Approximately the same numbers of the various cell populations were represented in the KC^{ERT} and *Gnat3*^{-/-};KC^{ERT} datasets (Figure 5A).

By comparing gene expression profiles of independent cell populations between KC^{ERT} and *Gnat3*^{-/-};KC^{ERT}

pancreata, we did not observe distinct expression profiles in the macrophage populations (Figure 5C). In contrast, MDSCs showed marked gene expression changes, with 56 genes being significantly altered between KC^{ERT} and *Gnat3*^{-/-};KC^{ERT} samples (Figure 5D). It was not possible to transcriptionally define gMDSCs and monocytic myeloid-derived suppressor cells (mMDSCs) with the same markers used for mass cytometry; therefore gene expression comparisons were done between all tumor infiltrating MDSCs in KC^{ERT} and *Gnat3*^{-/-};KC^{ERT} pancreata. Of interest, expression of the C-type lectin receptors, *Clec12a* and *Clec4a2*, were decreased in the *Gnat3*^{-/-};KC^{ERT} animals (Figure 5E). *Camp*,⁵⁰ *Ngp*, and *Ltf*,⁵¹ all associated with mature neutrophils, were decreased as well as *Pglyrp*⁵² and *Lyz2*,⁵³

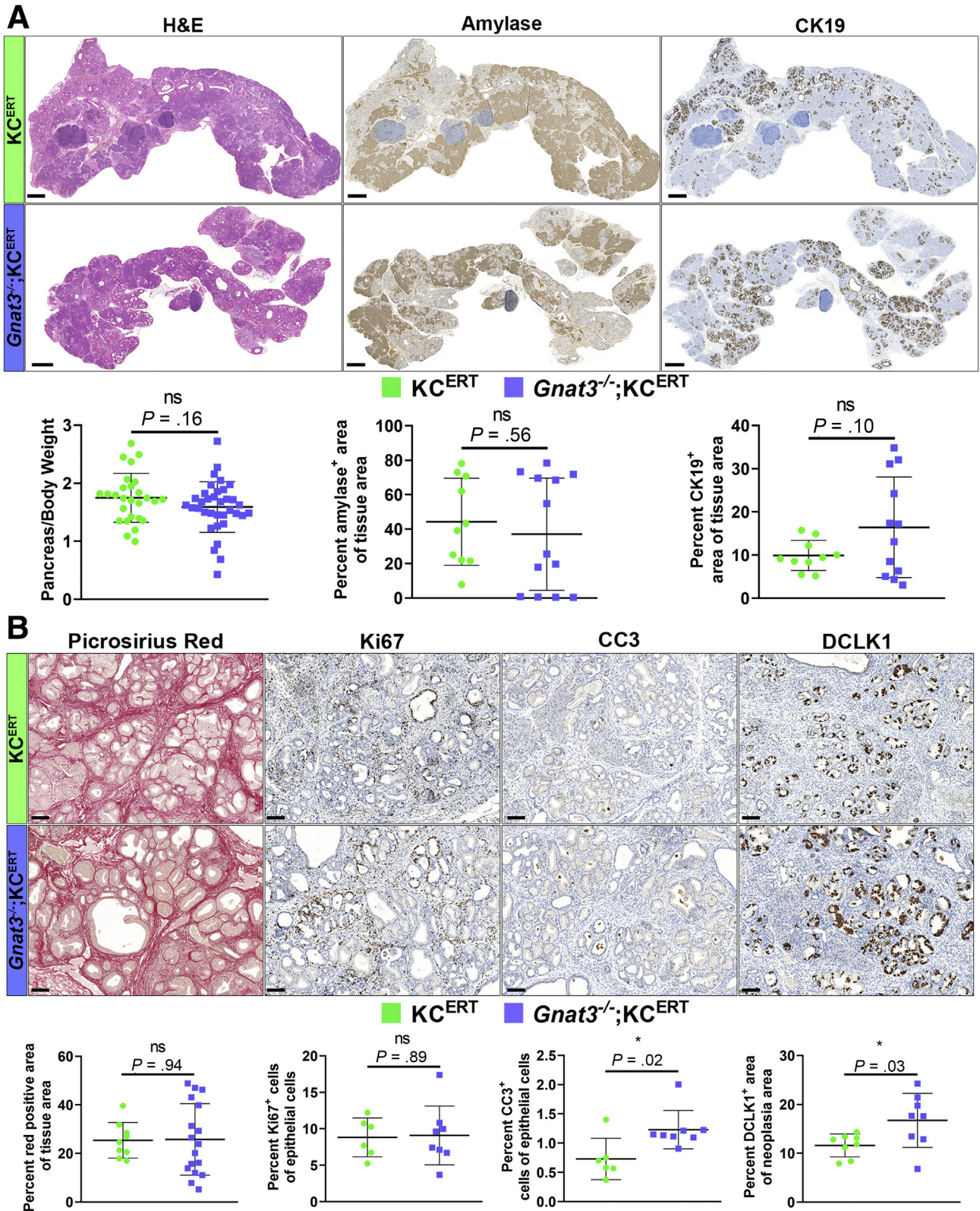


Figure 3. *Gnat3* ablation has no effect on pancreatic neoplasia formation. Analysis of tamoxifen and cerulein treated KC^{ERT} and *Gnat3*^{-/-};KC^{ERT} pancreata harvested 6 weeks after cerulein treatment. (A) H&E staining with pancreas-to-body weight ratios below (n = 27; 35). IHC for amylase (n = 10; 13) and CK19 (n = 10; 12) quantified below by total positive area from total pancreas area. Scale bars: 1000 μ m. (B) Staining for picrosirius red (n = 9; 17), Ki67, CC3 (n = 6; 8), and DCLK1 (n = 8) with quantification below for each. Scale bars: 100 μ m. Significance was calculated using an unpaired *t* test; $P < .05$ statistically significant.

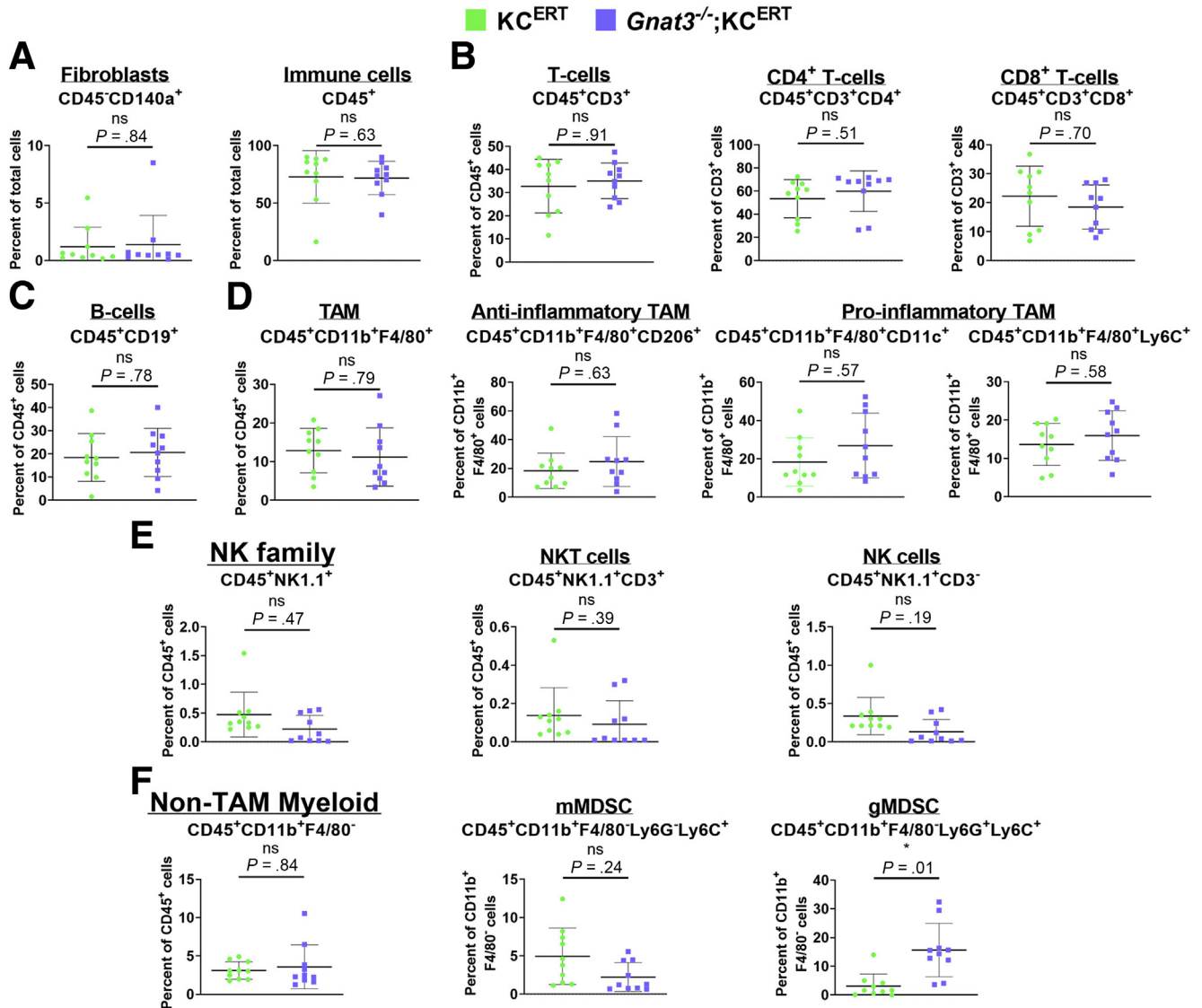


Figure 4. GNAT3 loss increases gMDSC presence during pancreatic transformation. Manually gated mass cytometry data from tamoxifen and cerulein treated KC^{ERT} and $Gnat3^{-/-};KC^{ERT}$ pancreata harvested 6 weeks after cerulein treatment ($n = 10$). (A) Percentage of fibroblasts ($CD140a^{+}$) or total immune cells ($CD45^{+}$) from total cell numbers. (B) T cells ($CD45^{+}CD3^{+}$) as percentage of total immune cells. Percent of $CD4^{+}$ T cells ($CD45^{+}CD3^{+}CD4^{+}$) and $CD8^{+}$ T cells ($CD45^{+}CD3^{+}CD8^{+}$) from T cells. (C) B cells ($CD45^{+}CD19^{+}$) as percent of total immune cells. (D) Percent of TAM ($CD45^{+}CD11b^{+}F4/80^{+}$) from total immune cells. TAM phenotypes were characterized by anti-inflammatory TAM ($CD45^{+}CD11b^{+}F4/80^{+}CD206^{+}$) and proinflammatory TAM ($CD45^{+}CD11b^{+}F4/80^{+}CD11c^{+}$ or $CD45^{+}CD11b^{+}F4/80^{+}Ly6C^{+}$) as percent of TAM. (E) NK family ($CD45^{+}NK1.1^{+}$) split into NK T cells ($CD45^{+}NK1.1^{+}CD3^{+}$) and NK cells ($CD45^{+}NK1.1^{+}CD3^{-}$) as percent of total immune cells. (F) Non-TAM myeloid cells ($CD45^{+}CD11b^{+}F4/80^{-}$) were determined as percent of total immune cells. MDSCs were separated into mMDSC ($CD45^{+}CD11b^{+}F4/80^{-}Ly6G^{+}Ly6C^{+}$) or gMDSC ($CD45^{+}CD11b^{+}F4/80^{-}Ly6G^{+}Ly6C^{-}$) populations as percent of non-TAM myeloid cells. Significance was calculated using the Mann-Whitney nonparametric test with Benjamini-Hochberg correction for multiple comparisons. P adjusted $< .05$ statistically significant.

known antimicrobial proteins, many of which are associated with proinflammatory responses (Figure 5E). Furthermore, although *Il1b*,⁵⁴ a known proinflammatory cytokine, was increased, many other immunomodulatory secreted proteins were decreased including *Serp1b1a*,⁵⁵ *Anxa1*,⁵⁶ and *Anxa3*,⁵⁷ suggesting an alteration in immune state and function (Figure 5E). Together with the previous mass cytometry data, single-cell RNA sequencing results suggest that *Gnat3* ablation in early neoplastic lesions

alters both the quantity and quality of the MDSC compartment.

Epithelial Expression of CXCL1 and CXCL2 Increase Upon GNAT3 Loss

We have found that ablation of GNAT3 alters MDSC immunomodulatory gene expression and increases gMDSC

numbers in the neoplastic pancreas as well as up-regulates CXCL1 and CXCL2, known regulators of MDSC recruitment and function,^{17,58} in organoid cultures (Figure 1E). CXCL1 and CXCL2 primarily signal through CXCR2 on immune cell populations and tumor cells to alter chemokine production, survival, and immune cell recruitment.^{26,59} Our single-cell RNA sequencing data showed *Cxcr2* expression localized in the MDSC population, indicating that MDSC function would be directly targeted by changes in CXCL1/2 expression (Figure 6A). Epithelial expression of *Cxcl1* and *Cxcl2* in the single-cell sequencing data was not informative because the numbers of epithelial cells were too few to compare because our tissue digestion conditions were optimized for retrieval of immune cells and fibroblasts.⁶⁰

To characterize CXCL1 and CXCL2 levels in *Gnat3*^{-/-};KC^{ERT} animals, we used IHC, enzyme-linked immunosorbent assay (ELISA) and in situ hybridization assays. Our results showed that CXCL1 IHC did not differ in stromal cells but was increased in neoplastic lesions in *Gnat3*^{-/-};KC^{ERT} mice, consistent with our ex vivo culture system (Figure 6B). Lacking a CXCL2 antibody suitable for IHC, we measured protein levels in lysates from small fragments of pancreatic tissue by ELISA. We found a trend toward higher CXCL2 protein in *Gnat3*^{-/-};KC^{ERT} animals (Figure 6C), which did not reach statistical significance. We then used RNAscope in situ hybridization to detect *Cxcl2* expression. *Cxcl2* transcripts were expressed focally, with some areas showing many cells with robust expression and others having virtually none, potentially explaining the variability in our ELISA results (Figure 6D). After quantitation of *Cxcl2* puncta, we found that expression levels were higher in both the stroma and neoplastic compartment in *Gnat3*^{-/-};KC^{ERT} mice (Figure 6D). Additional analysis of the single-cell RNA sequencing data found expression of *Cxcl1* or *Cxcl2* primarily in fibroblasts or TAM/MDSC, respectively, in both KC^{ERT} and *Gnat3*^{-/-};KC^{ERT} mice (Figure 6E and F). However, in these experiments, tissue digestion was performed to enhance recovery of cells within the fibroinflammatory stroma and may have missed MTCs in the underrepresented epithelial population.

To analyze expression of CXCL1 and CXCL2 by MTC, we probed single-cell RNA sequencing data from KC animals, increasing the number of epithelial cells collected for analysis. Unsupervised clustering via UMAP was performed and characterized, identifying a small but distinct MTC population as indicated by coexpression of the tuft cell markers *Dclk1*, *Vav1*, and *Pou2f3* (Figure 7A–C). We found low to no expression of *Cxcl1* or *Cxcl2* (Figure 7C) in the MTCs, with both primarily expressed by non-epithelial cell types. However, these data do not preclude the possibility that *Gnat3*-ablated MTCs acquire the ability to make CXCL1/2. To address this possibility, for CXCL1, we used co-immunofluorescence to stain KC^{ERT};ROSA26^{L^{SL}-EYFP} and *Gnat3*^{-/-};KC^{ERT};ROSA26^{L^{SL}-EYFP} pancreata, where YFP expression marks acinar-derived daughter cells and COX1 was used as a MTC marker. Once again, the most intense CXCL1 staining in control KC^{ERT};ROSA26^{L^{SL}-EYFP} mice was found primarily in YFP-negative non-epithelial cells (Figure 7D, white arrows). In *Gnat3*^{-/-};KC^{ERT};ROSA26^{L^{SL}-EYFP}

mice, epithelial cells also begin to express CXCL1 (Figure 7D, purple arrows), with MTCs expressing relatively low levels (Figure 7D, yellow arrows). Taken together, our data show that tissues from *Gnat3*^{-/-};KC^{ERT} mice have increased levels of CXCL1 with a smaller, but still significant, change in *Cxcl2* expression, both of which can stimulate CXCR2 on MDSCs, consistent with an increase in infiltration of this population.

Gnat3 Ablation Accelerates Progression to Metastatic Pancreatic Cancer

Our data suggest that MTC chemosensory signaling does not play a substantial role during the onset of pancreatic tumorigenesis but does influence the immune-suppressive microenvironment. Because of the increased pro-tumor gMDSC population in *Gnat3*^{-/-};KC^{ERT} pancreata through the CXCL1/2-CXCR2 axis, we hypothesized that overall tumor progression would be enhanced by *Gnat3* ablation. To address the long-term effects of *Gnat3* ablation, we turned to the well-established KC model of pancreatic neoplasia. KC and *Gnat3*^{-/-};KC mice were aged until moribund, with the experiment terminated at 52 weeks. Within this time frame, KC mice rarely progress to PDA, generally presenting with advanced PanIN lesions and a substantial fibroinflammatory stromal reaction.⁶¹ Consistent with this, only 1 KC mouse in our cohort became moribund before the endpoint of the experiment. In contrast, 30% of *Gnat3*^{-/-};KC mice became moribund and required euthanasia before 52 weeks of age (Figure 8A). Assessment of pancreatic histology confirmed that 4 of 12 control KC mice had histopathologically detectable focal lesions of early stage adenocarcinoma, primarily moderately to well-differentiated with local stroma invasion, whereas 11 of 16 *Gnat3*^{-/-};KC mice had progressed to aggressive PDA, with 5 having extensive primary tumor mass (Figure 8B). Tumor grading indicated that *Gnat3*^{-/-};KC animals had more high-grade tumors, evident in sarcomatoid carcinoma and poorly differentiated carcinoma in 3 of the *Gnat3*^{-/-};KC mice (Figure 8C). Comparing CK19 IHC, a marker of ductal transformation, between KC and *Gnat3*^{-/-};KC tissue illustrated the difference in histology as well as a distinct sarcomatoid tumor in the *Gnat3*^{-/-};KC mice, noted by the absence of CK19 stain (Figure 8D).

Finally, 4 *Gnat3*^{-/-};KC animals had frank macrometastasis to liver or lung on dissection, marked by CK19 positivity, with none of the KC mice showing distant metastatic spread (Figure 8E). Analysis of CXCL1 IHC and *Cxcl2* in situ hybridization also showed a trend toward higher levels in *Gnat3*^{-/-};KC tissue, with staining being more prominent in areas that had progressed to carcinoma (Figure 8F and G). Because progression to carcinoma was a more common outcome in the *Gnat3*^{-/-};KC mice, the higher levels of CXCL1/2 may be a secondary effect of the accelerated tumor progression. In total, our data suggest that MTC chemosensation serves to limit the immune-suppressive microenvironment in part by tempering the expression of CXCL1/2, thus slowing PDA progression.

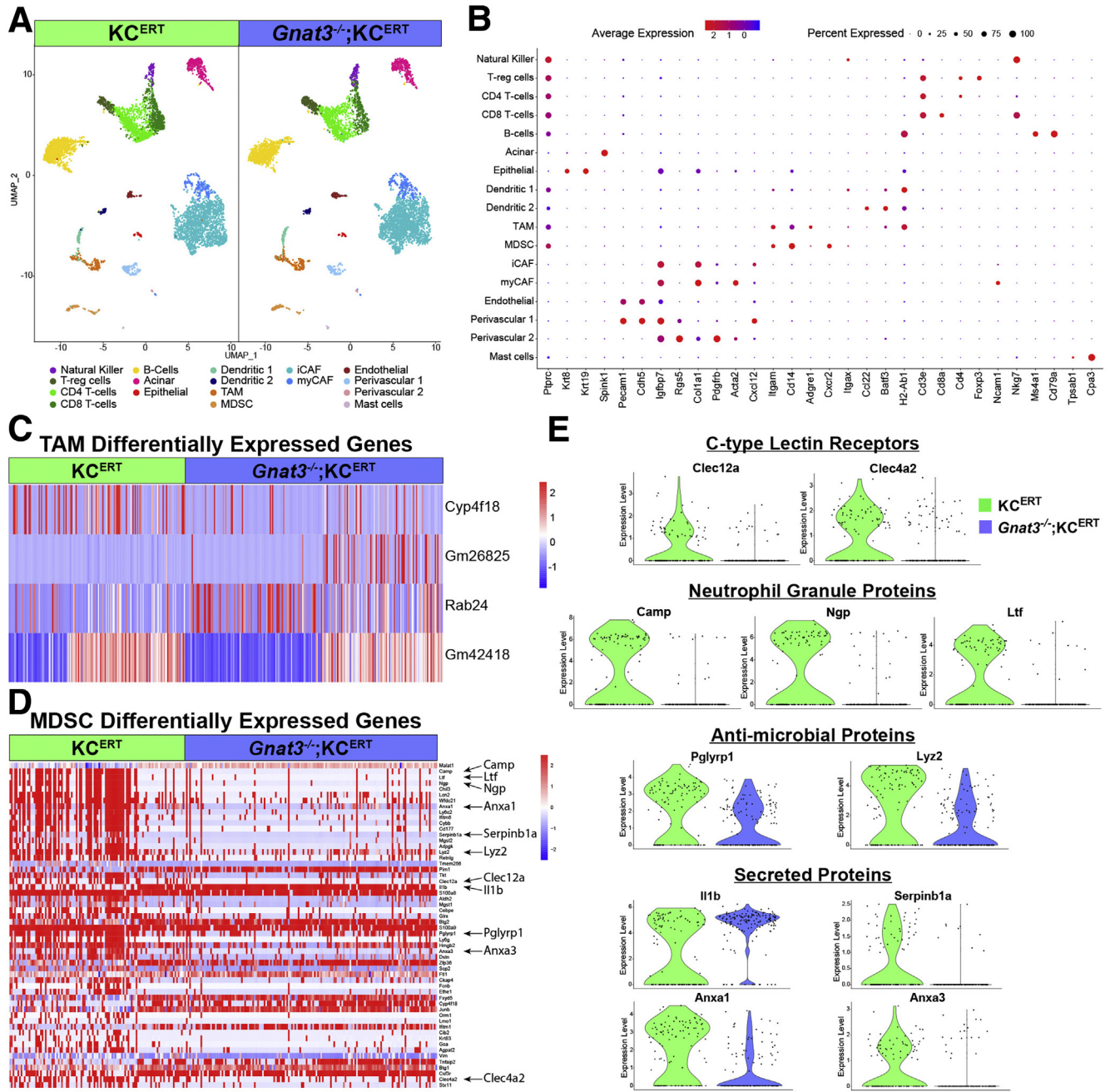


Figure 5. Single-cell RNA transcriptomic analysis identifies altered MDSC gene expression in *Gnat3* ablated neoplasia. Analysis of tamoxifen and cerulein treated KC^{ERT} and *Gnat3*^{-/-};KC^{ERT} single-cell RNA transcriptomes from pancreata collected 6 weeks after cerulein treatment. (A) Unbiased clustering of single cells driven by transcriptome differences and visualized by UMAP (n = 2; 2). (B) Dot plot of gene expression patterns used to identify cell populations from pooled KC^{ERT} and *Gnat3*^{-/-};KC^{ERT} cells. Percent of cells expressing each gene per cluster noted by dot size. Average gene expression is represented by color of dot. iCAF, inflammatory cancer associated fibroblasts; myCAF, myofibroblastic cancer associated fibroblasts; T-reg, T regulatory cells. (C and D) Heatmap of single-cell RNA transcriptomes for TAMs (C) and MDSCs (D) displaying the statistically significant differentially expressed genes (rows). Selected genes identified on right of MDSC heatmap. (E) Violin plots displaying frequency and expression levels of selected genes from cells in the MDSC cluster. Genes labeled by group: C-type lectin receptors (*Clec12a*, *Clec4a2*), neutrophil granule proteins (*Camp*, *Ngp*, *Ltf*), antimicrobial proteins (*Pglyrp1*, *Lyz2*), and secreted proteins (*Il1b*, *Serpinb1a*, *Anxa1*, *Anxa3*). Significance was calculated using Bonferroni adjusted *P* values from nonparametric Wilcoxon rank sum test. *P* adjusted < .05 statistically significant.

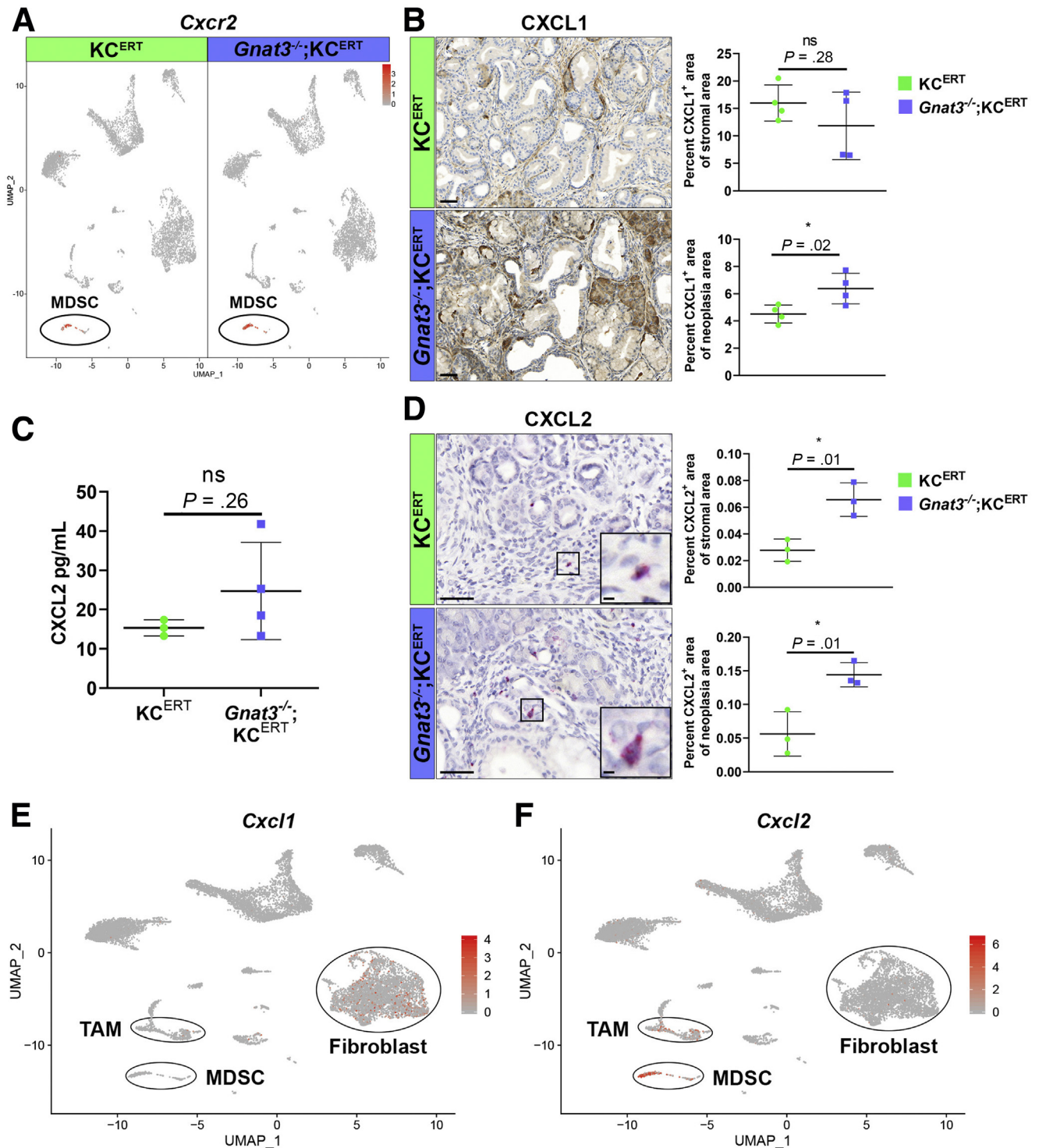


Figure 6. *Gnat3* ablation increases CXCL1 and CXCL2 expression in the neoplastic epithelial compartment. Analysis of tamoxifen and cerulein treated KC^{ERT} and $Gnat3^{-/-};KC^{ERT}$ pancreata collected 6 weeks after cerulein treatment. (A) UMAP of *Cxcr2* single-cell RNA transcriptome expression from KC^{ERT} and $Gnat3^{-/-};KC^{ERT}$ cells. MDSC cluster circled. Color scale denotes expression level. (B) IHC for CXCL1 quantified from positive area of stroma or neoplasia area ($n = 4$). Scale bar: 50 μ m. (C) CXCL2 protein levels measured by ELISA from pancreas lysate ($n = 3; 4$). (D) In situ hybridization for *Cxcl2* transcript quantified by positive puncta area (red) of stroma or neoplasia area ($n = 3$). Inset boxes are magnified area. Scale bar: 50 μ m, inset = 5 μ m. (E and F) UMAP of single-cell RNA transcriptome expression from pooled KC^{ERT} and $Gnat3^{-/-};KC^{ERT}$ data where gene expression is denoted by red per each cell for *Cxcl1* (E), primarily in fibroblasts, and *Cxcl2* (F), primarily in TAM and MDSC compartments as circled. Significance was calculated using an unpaired *t* test; $P < .05$ statistically significant.

Discussion

MTCs are present in both human and mouse cancers and have been hypothesized to have multiple roles contributing to tumor progression, such as a quiescent stem-like population^{62–64} or an immune modulatory sensory cell.²⁴ Previous studies in our laboratory identified MTCs in the neoplastic pancreas that expressed components of the chemosensory signaling cascade,^{19,30} suggesting that these cells can sense and respond to stimuli. To assess whether MTC chemosensation can drive pancreatic tumor progression, we used a KRAS-initiated model of pancreatic neoplasia and ablated *Gnat3*, the gene that encodes α -gustducin, a gustatory pathway G-protein expressed specifically in normal tuft cells, MTCs, and type II cells of taste buds. To our surprise, we found that GNAT3 functions to restrict rather than promote PDA progression.

We found no difference in transformation on ablation of *Gnat3* but did find changes in MDSC immune regulatory gene expression as well as a specific increase in the infiltration of tumor-promoting gMDSCs.¹⁷ Furthermore, CXCL1 and CXCL2 expression was increased in epithelial cells both in vivo and ex vivo. Together, these data suggest that GNAT3, and by extension MTCs, limits the immunosuppressive microenvironment, thus slowing PDA progression. Indeed, we found that *Gnat3*-ablated KC mice progressed rapidly to metastatic PDA, indicating a pivotal role of MTC sensory function in suppressing PDA progression.

Up-regulation of CXCR2 ligands, such as CXCL1, CXCL2, and CXCL5, in human specimens and mouse models of PDA correlate with decreased survival and morbidity.^{17,26,27} Functional studies of CXCL1/2 signaling to CXCR2 on MDSCs activate and increase gMDSCs in the tumor microenvironment.^{17,26,27,35} Activated gMDSCs enhance immunosuppression by releasing reactive oxygen species and arginase 1,⁶⁵ suppressing the tumor mediated cytotoxicity and influx of CD4⁺ and CD8⁺ T cells, which promotes PDA progression and metastatic spread.^{47,66} Our data show *Gnat3* ablation increases expression of CXCL1/2 by epithelial cells and alters immunomodulatory gene expression in *Cxcr2*-expressing MDSCs, with increased infiltrating gMDSC numbers. We found no difference in number and only slight differences by gene expression in T-cell response with *Gnat3* ablation, possibly because of the early stage of lesions analyzed. Our data also found accelerated tumor progression, resulting in advanced tumor grade and metastasis with long-term *Gnat3* loss in KC mice, consistent with tumor cell CXCL1/2 activating CXCR2 on MDSCs and neutrophils promoting metastatic PDA.^{26,35}

The ablation of gustatory signaling alters the ability of normal tuft cells to sense and respond to luminal signals.²⁴ Loss of sensory signals diminishes secondary responses including lack of action potentials in secondary nerves from type II taste cells on the tongue³⁰ as well as lack of acetylcholine signaling to promote immune responses in the nasal epithelium.^{21,29,67} In the intestine, loss of gustatory signaling prevents small intestinal tuft cell hyperplasia and blocks release of interleukin 25 after parasitic infection, inhibiting parasite expulsion.^{22,23} Surprisingly, our data

show that *Gnat3* loss increases the release of specific cytokines by epithelial cells within the neoplastic pancreas. It is possible that the loss of MTC sensation may lead to uncontrolled release of intracellular cargo, directly explaining the increased cytokine levels, a condition that would be further exacerbated by the larger number of tuft cells that form after *Gnat3* ablation. However, it seems more likely that this is a secondary effect caused by the loss of MTC function acting on surrounding cells, a possibility supported by our observation that CXCL1 and CXCL2 levels are higher in non-MTC epithelia and stromal cells in the GNAT3 null background (Figure 6B). Indeed, while the current manuscript was in revision, Delgiorno et al⁶⁸ have reported that tuft cell ablation accelerates pancreatic tumor progression, supporting our interpretation that knocking out *Gnat3* leads to loss of MTC function.

In summary, our data support that MTCs use gustatory signaling to suppress PDA progression in part by suppressing the CXCL1/2-CXCR2 immunomodulatory signaling axis, although other cytokines may also play a role in this response. This suggests the intriguing possibility that stimulation of the bitter/umami taste sensory pathway may further suppress PDA progression. If this stimulation were to further limit the immune-suppressive microenvironment, it may be an effective method to enhance the responsiveness to immune therapies in the treatment of pancreatic cancer.

Methods

Mice

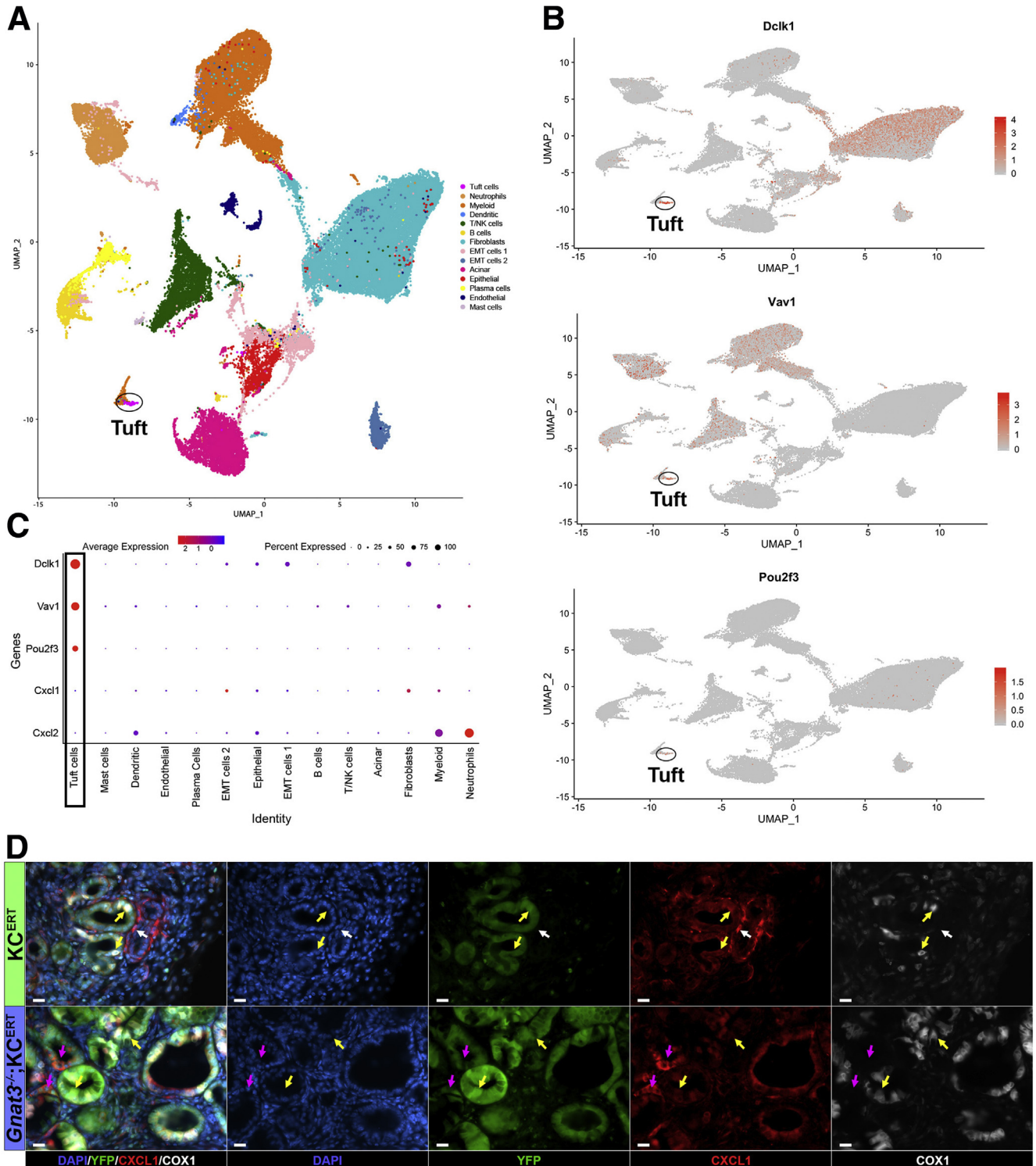
All animal procedures and experiments were conducted with approval of the Institutional Committee on Use and Care of Animals at the University of Michigan. The following mice strains were used: *Ptf1a*^{Cre/+} and *Ptf1a*^{CreERT/+69}; *Kras*^{G12D/+} (gift of David Tuveson, Cold Spring Harbor Laboratory, NY), *Gnat3*^{-/-} (gift of Robert Margolskee, Monell Chemical Senses Center, PA),²⁹ and ROSA26^{LSL-EYFP}. Mice were crossed on a mixed background to generate *Gnat3*^{-/-}; *Kras*^{G12D/+}; *Ptf1a*^{Cre/+} and *Gnat3*^{-/-}; *Kras*^{G12D/+}; *Ptf1a*^{CreERT/+} mice. All analyses were performed by using strain-controlled animals. Analysis of adult pancreata was performed by using 8- to 52-week-old WT or *Gnat3*^{-/-} mice. Aged *Kras*^{G12D/+}; *Ptf1a*^{Cre/+} and *Gnat3*^{-/-}; *Kras*^{G12D/+}; *Ptf1a*^{Cre/+} mice were monitored and euthanized at moribund per animal care guidelines.

Acinar specific *Kras*^{G12D/+} recombination was induced in 8- to 12-week-old *Kras*^{G12D/+}; *Ptf1a*^{CreERT/+} mice by oral gavage with 5 mg tamoxifen (T5648; Millipore-Sigma, St Louis, MO) dissolved in corn oil for 5 days. After a 2-day rest after tamoxifen treatment, experimental pancreatitis was induced once a day by intraperitoneal injection with 250 μ g/kg cerulein (46-1-50; American Peptide Company, Inc, Sunnyvale, CA) for 5 days. Pancreata were harvested either 1 or 6 weeks after cerulein treatment. Experimental pancreatitis was also induced by 8 hourly intraperitoneal injections of 75 μ g/kg cerulein (46-1-50; American Peptide Company) in a 5-week-old *Kras*^{G12D/+}; *Ptf1a*^{Cre/+} animal that was collected and sequenced at 16-weeks-old (Figure 7A–C).

Immunohistochemistry and Quantification

Pancreata were collected, weighed, and fixed in Z-fix (NC9050753; Anatech Ltd, Battle Creek, MI) overnight. Processing of tissues was performed by using a Leica ASP300S tissue processor (Buffalo Grove, IL). Sections (4

µm) of paraffin-embedded tissue were stained for target proteins by using the Discovery Ultra XT autostainer (Ventana Medical Systems Inc, Tucson, AZ). Antibodies were stained as depicted in Table 1, followed by Mayer's hematoxylin (NC9220898; Millipore-Sigma) counterstain. H&E



staining was done by using Mayer's hematoxylin-eosin Y (HT110116; Fisher, Pittsburgh, PA). Histopathologic quantification of H&E staining was performed by pathologists (YZ, WY) on de-identified images using an Olympus BX53F microscope (Olympus, Shinjuku City, Tokyo, Japan), as previously described.⁷⁰ Macrometastasis presence in the liver and lung was determined by visual inspection and confirmed by H&E. Picrosirius red staining was performed on sectioned paraffin-embedded tissue per manufacturer's instructions (Polysciences Inc, Warrington, PA). IHC slides were imaged and stitched together by a Panoramic SCAN scanner (Perkin Elmer, Seattle, WA) using a $\times 20$ objective lens.

Scanned images were quantified by using Halo software (Indica Labs, Corrales, NM) algorithms to analyze the stitched pancreas slide images using the entire pancreas area as the total area of comparison for staining, following the exclusion of blood vessels, lymph nodes, and adipose/connective tissue. Utilization of Halo algorithms allows the training of the software to identify tissue architecture via histology to separate stroma, neoplastic, and acinar compartments for analysis and compare staining area per compartment. Quantification of DCLK1 staining used the area of all neoplastic lesions per scanned pancreas image and determined the percentage of the positive brown stain (Figures 2B and 3B). Similarly, analysis of Ki67 and CC3 identified the total cell number by blue hematoxylin stain in the neoplastic and acinar compartments to determine the percentage of positive brown staining cells in those compartments (Figure 3B). Quantification of CK19, amylase, or picrosirius red staining was found as a percentage of brown or red positive area, respectively, of total pancreas area (Figure 3A and B). In Figure 6B and D, CXCL1 and *Cxcl2* positive stains were quantified by the percentage of brown or red staining, respectively, in the neoplastic or stromal compartments. Analysis of CXCL1 and *Cxcl2* percent positive staining area in Figure 8F and G was performed from total pancreas area without separation by compartment, because tissue architecture following carcinoma makes clear separation of cell compartments not possible for quantification algorithms.

Tissue Immunofluorescence

Immunofluorescence staining was performed on frozen tissue sections, as described previously.⁷¹ In sum, pancreata

were collected and fixed in Z-fix for 2–3 hours, followed by 30% sucrose in phosphate-buffered saline (PBS) overnight. Pancreata were equilibrated in a 1:1 mixture of 30% sucrose/PBS and optimal cutting temperature embedding medium for 30 minutes, embedded in optimal cutting temperature embedding medium, frozen by liquid nitrogen, and stored at -80°C . Frozen tissue sections ($10\ \mu\text{m}$) were acquired by using a Leica CM1860 (Leica Biosystems, Buffalo Grove, IL) cryostat set at -20°C , permeabilized in 0.1% Triton X-100 (T9284; Millipore-Sigma) in PBS for 1 hour, and blocked by using 5% donkey serum/1% bovine serum albumin (BSA) in PBS for 1 hour. Incubation with primary antibody (listed in Table 1) was performed overnight at room temperature in 0.1% Triton X-100/1% BSA in PBS, followed by 3 washes of 0.1% Triton X-100/PBS for a total of 45 minutes. Sections were incubated with Alexa Fluor-conjugated secondary antibodies at 1:500 and phalloidin at 1:250 (both Invitrogen, Carlsbad, CA) for 1 hour at room temperature, followed by 3 washes as before. Finally, slides were rinsed in deionized water and mounted with Prolong Diamond antifade mountant (P36961; Fisher). Images were acquired on a LSM800 confocal microscope (Zeiss, Oberkochen, Germany) using a $\times 63$ objective.

Organoid Culture

Acinar cell isolation from fresh pancreas was performed as previously described.⁷² Briefly, pancreata from 8- to 10-week-old mice were sterilely harvested, washed twice in Hank's buffered salt solution (HBSS), minced, and digested in 0.2 mg/mL Collagenase P (11249002001; Millipore-Sigma) for 15 minutes at 37°C . Tissue was washed 3 times in 5% fetal bovine serum (FBS) in HBSS, centrifuged at 300g for 2 minutes, resuspended in HBSS, and filtered through 500 μm and 105 μm polypropylene mesh (888-13570 and 888-13597; Spectrum Laboratories, New Brunswick, NJ). Cell suspension was slowly added to a gradient consisting of 30% FBS in HBSS and centrifuged at 300g for 2 minutes. Cells were resuspended in PTOM, made as previously described with 100 U/mL Pen Strep (15140122; Invitrogen), 1% B27 supplement (17504044; Invitrogen), 50 $\mu\text{g}/\text{mL}$ ascorbic acid (A4403; Millipore-Sigma), 0.4% bovine pituitary extract (13028-014; Thermo Fisher, Waltham, MA), 10 $\mu\text{g}/\text{mL}$ insulin (I2643; Millipore-Sigma), 0.5 $\mu\text{g}/\text{mL}$ hydrocortisone (H0888; Millipore-Sigma), 5 ng/mL FGF-2 (F0291; Millipore-Sigma), 10 ng/

Figure 7. (See previous page). Single-cell sequencing of pancreata identifying a tuft cell specific gene cluster. Analysis of KC single-cell RNA transcriptomes. (A) Unbiased clustering of single cells driven by transcriptome differences and visualized by UMAP. MTC cluster is circled. EC, endothelial cells. (B) UMAP of tuft cell markers *Dclk1*, *Vav1*, and *Pou2f3* single-cell RNA transcriptome expression from KC cells with MTC cluster circled. Color scale denotes expression level. (C) Dot plot of gene expression patterns for MTC markers *Dclk1*, *Vav1*, and *Pou2f3* as well as *Cxcl1* and *Cxcl2* expression per cell populations from KC cells. MTC cluster is outlined with other cell populations indicated beneath. Percent of cells expressing each gene per cluster is noted by dot size. Average gene expression is represented by color of dot. (D) Co-immunofluorescence for CXCL1 (red) and MTC marker COX1 (white) in tamoxifen and cerulein treated KC^{ERT};ROSA26^{LSL-EYFP} and *Gnat3*^{-/-};KC^{ERT};ROSA26^{LSL-EYFP} pancreata collected 6 weeks after cerulein treatment. In KC^{ERT};ROSA26^{LSL-EYFP} pancreata a high level CXCL1 expression (red) is found primarily in non-epithelial cells (YFP⁻, white arrows) and low expression in MTCs (YFP⁺, COX1⁺, yellow arrows). In *Gnat3*^{-/-};KC^{ERT};ROSA26^{LSL-EYFP}, non-MTC epithelia (YFP⁺, COX1⁻, purple arrows) express high levels of CXCL1, whereas relatively low expression is found in MTCs (yellow arrows) and in stromal cells. DAPI (blue) counterstains nuclei. Scale bar: 20 μm .

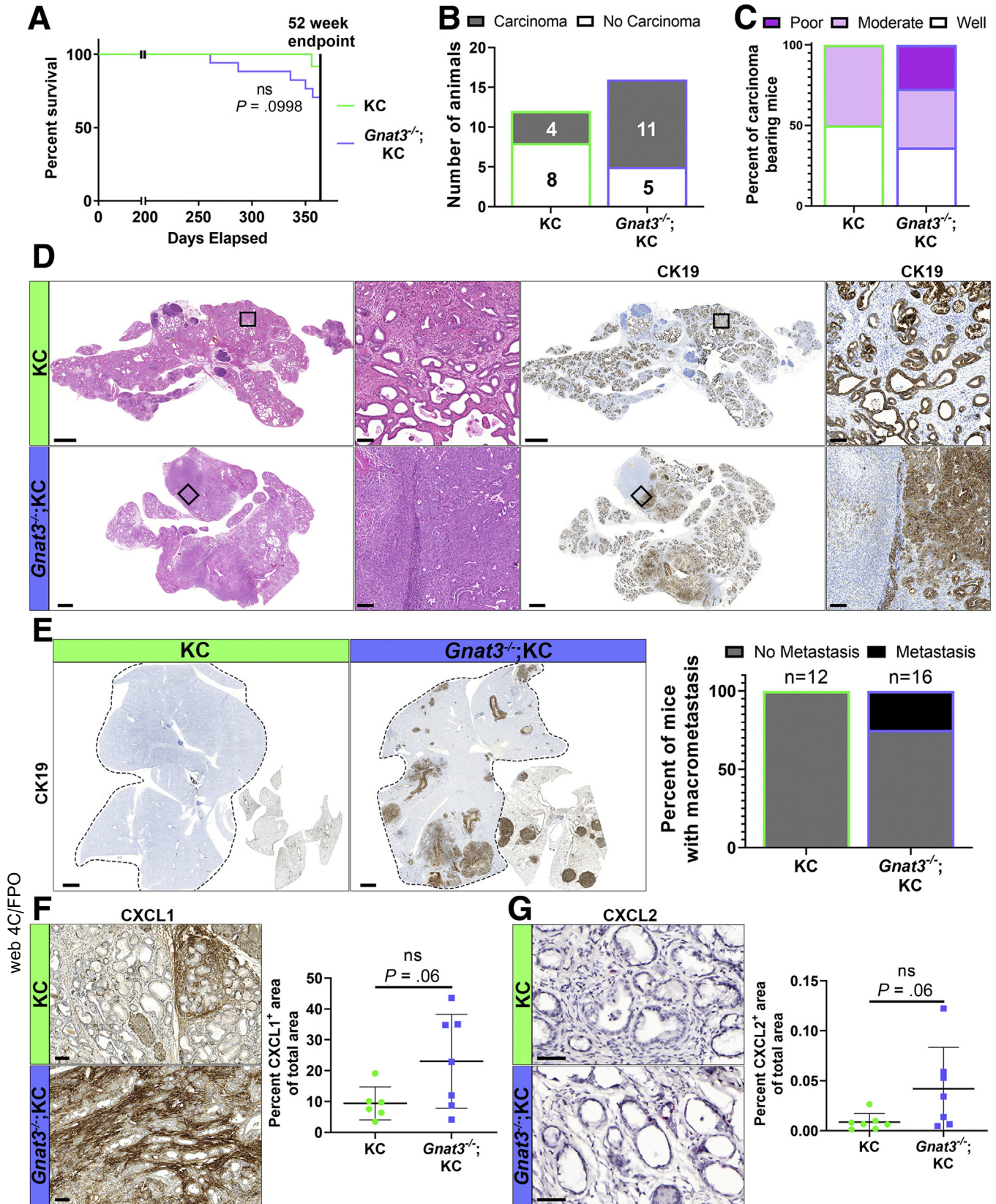


Table 1. Antibodies Used for Immunocytochemistry

Antibody	Company	Catalog number	Lot number	Dilution	Purpose
DCLK1	Abcam	ab37994	GR3202231-1	1:2000	IHC, IF
VAV1	Cell Signaling	2502S	2	1:100	IF
GNAT3	Abcam	ab113664	GR252824-10	1:250	IF
COX1	Santa Cruz	sc-1754	L1312	1:200	IF
COX2	Santa Cruz	sc-1747	C1211	1:200	IF
Amylase	Sigma-Aldrich	A8273	075K4833	1:1000	IHC
Cytokeratin 19	Abcam	ab133496	GR119187-5	1:500	IHC
Ki67	Abcam	ab15580	827779	1:1000	IHC
Cleaved caspase 3	Cell Signaling	9664L	22	1:100	IHC
CXCL1	Abcam	ab86436	GR3203782-23	1:100	IHC, IF

IF, immunofluorescence.

mL FGF-10 (345-FG; R&D Systems, Minneapolis, MN), 25 nmol/L retinoic acid (R2625, Millipore-Sigma), and 5 μ mol/L Y-27632 (50-175-996; Fisher) in Dulbecco modified Eagle medium:Glutamax (10564-011; Thermo Fisher).³¹ Acinar cells were floated in a petri dish for 2 hours in PTOM, and then 10,000–12,500 cells were plated in a PTOM 5% Matrigel mixture on a bed of 100% Matrigel in a 24-well plate. Medium was changed to fresh PTOM every 4 days.

Organoid Culture Immunofluorescence and Counting

Organoids were fixed and stained by using a modified protocol previously described.⁷³ In sum, after a PBS wash, the organoids were fixed in Z-fix for 15 minutes, washed twice in PBS, and permeabilized in 0.5% Triton X-100/PBS for 1 hour. After a second wash, organoids were blocked in 10% FBS/1% BSA in PBS for 1 hour and then incubated with the primary antibody (VAV1, as in Table 1) in 1% FBS/1% BSA in PBS overnight at 4°C. Organoids were washed 3 times in 1% FBS/1% BSA/PBS for a total of 45 minutes and then incubated with an Alexa Fluor-conjugated secondary antibody at 1:500 and phalloidin at 1:250 (both Invitrogen) in 1% FBS/1% BSA/PBS for 2 hours. Organoids were washed for 30 minutes in 3 changes of PBS, carefully removed intact from their 24-well plates, and mounted on a slide with Prolong Diamond antifade mountant (P36961; Fisher). Finally, the slides were compressed overnight at room temperature. The number of organoids and number of tuft cells per organoid per well were counted per slide by using an Olympus IX83 Inverted Microscope (Olympus). Each biological sample had between 3 and 6 wells counted, with a minimum of 77 and up to 165 organoids counted per

sample. Organoid cultures were collected at 35, 26, and 20 days after acinar plating.

Cytokine Array

Conditioned media were collected from KC and *Gnat3*^{-/-};KC organoid cultures, pooled from 6 wells, centrifuged at 5000 RPM for 15 minutes to remove debris, and stored at -80°C for later analysis using the Mouse XL Cytokine Array Kit (ARY028; R&D Systems) per manufacturer's instructions. The biological triplicate data in Figure 1E were carried out by using conditioned media collected at day 32 (for 2 repeats) and day 20 (for 1 repeat). Briefly, membranes were washed with Array Buffer 6 for 1 hour, and then 560 μ l or 630 μ l conditioned medium was added, plus array buffer mix, to membranes and incubated overnight at 4°C. Membranes were washed 3 times for a total of 30 minutes in 1 \times Wash Buffer before adding Detection Antibody Cocktail in the array buffer mix for 1-hour incubation. Washing was repeated, and then streptavidin-horseradish peroxidase was incubated for 30 minutes after washing and incubation with the ChemiReagent Mix. The chemiluminescent signal on the membranes was detected and analyzed by the Bio-Rad ChemiDoc Imaging System and Bio-Rad image Lab software version 6.0.1, respectively (Bio-Rad Laboratories, Hercules, CA). The volume tool was used to make a 1.4-mm² circle around each antibody detected spot to acquire the pixel density means of each dot, subtracted from a blank image area. The pixel density means were imported into Microsoft Excel 2016 (Redmond, WA) and subtracted from the blank signal, and each duplicate spotted pair was averaged to get a final value. The

Figure 8. (See previous page). Ablation of *Gnat3* increases PDA genesis, grade and metastasis. Analysis of KC and *Gnat3*^{-/-};KC mice aged to moribund or 52 weeks. (A) Kaplan-Meier survival curve, with endpoint of study indicated by black line at 52 weeks (n = 12; 17). (B and C) H&E analysis of tissues to determine number of mice with carcinoma (n = 12; 16) (B) and grading of carcinoma samples (poor, moderate, or well) (n = 4; 11) (C). (D) H&E and IHC for CK19. Inset boxes are magnified area. Scale bar: full pancreas = 2000 μ m, inset = 100 μ m. (E) IHC for CK19 on KC or *Gnat3*^{-/-};KC lung and liver (black dashed line) and quantification of mice with macrometastasis (n = 12; 16). Scale bar: 2000 μ m. (F) IHC for CXCL1 on KC or *Gnat3*^{-/-};KC pancreas quantified by positive stain from total pancreas area (n = 6; 7). Scale bar: 100 μ m. (G) In situ hybridization for *Cxcl2* transcript quantified by positive puncta area (red) of total pancreas area from KC or *Gnat3*^{-/-};KC pancreata (n = 7, 7). Scale bar: 50 μ m. Significance was calculated using the log-rank (Mantel-Cox) test and unpaired *t* tests; *P* < .05 statistically significant.

Table 2. Antibodies Used for Mass Cytometry

Antibody	Label	Catalog number	Dilution	Clone
CD140a	148Nd	3148018B	1:100	APA5
CD31 (PECAM-1)	165Ho	3165013B	1:100	390
CD45	089Y	3089005B	1:200	30-F11
CD19	149Sm	3149002B	1:200	6D5
CD161 (NK1.1)	170Er	3170002B	1:100	PK136
CD3e	152Sm	3152004B	1:100	145-2C11
CD4	145Nd	3145002B	1:200	RM4-5
CD8a	168Er	3168003B	1:200	53-6.7
FoxP3	158Gd	3158003A	1:100	FJK-16s
TCR $\gamma\delta$	159Tb	3159012B	1:100	GL3
CD11b (Mac-1)	143Nd	3143015B	1:300	M1/70
CD11c	209Bi	3209005B	1:100	N418
F4/80	146Nd	3146008B	1:100	BM8
CD206 (MMR)	169Tm	3169021B	1:200	C068C2
Ly-6G	141Pr	3141008B	1:400	1A8
Ly-6C	150Nd	3150010B	1:400	HK1.4

corresponding signals were then obtained by normalizing the pixel density of *Gnat3*^{-/-};KC with KC.

Mass Cytometry Immune Phenotyping

Mouse pancreata were collected, minced, washed in PBS, and then digested by using 1 mg/mL of collagenase type V (C9263; Millipore-Sigma) in RPMI medium at 37°C with gentle shaking for 15 minutes. Samples were washed with 10% FBS/RPMI 3 times and then filtered through 500 μ m, 105 μ m (888-13570 and 888-13597; Spectrum Laboratories), and 40 μ m filters (22-363-547; Fisher) to obtain single cells. Isolated single cells were prepared for mass cytometry according to manufacturer's instructions, as previously described.⁷⁴ Briefly, single cell suspensions were washed twice with MaxPar PBS (201058; Fluidigm, San Francisco, CA) before Cell-IDTM Cisplatin Live/Dead staining (201194; Fluidigm). Cell-IDTM Cisplatin reagent (1.67 μ mol/L) was incubated for 5 minutes and quenched by adding 4 mL of MaxPar Cell Staining Buffer (201068; Fluidigm), followed by centrifugation at 300g for 5 minutes. Supernatant removal was followed by 2 mL wash of MaxPar Cell Staining Buffer. Up to 3 million cells per sample were stained with cell surface antibody cocktail (all antibodies from Fluidigm in Table 2) in 100 μ L volume of MaxPar Cell Staining Buffer for 30 minutes, followed by 2 washes in MaxPar Cell Staining Buffer. Cell fixation was achieved by addition of freshly prepared 1.6% methanol-free formaldehyde (28906; Thermo Fisher) in MaxPar PBS for 10 minutes. After fixation, samples were washed once with MaxPar Cell Staining Buffer, incubated with MaxPar Nuclear Antigen Staining Buffer (201063; Fluidigm) for 15 minutes, washed twice with MaxPar Nuclear Antigen Staining Perm (201063; Fluidigm), and then an intracellular antibody (FoxP3, in Table 2) was added for 30-minute incubation. After a wash in MaxPar Nuclear Antigen Staining Perm and a wash in 2 mL MaxPar Cell Staining Buffer, cells were resuspended in 2

mL of 125 nmol/L Cell-ID Intercalator-Ir (201192B; Fluidigm) solution in MaxPar Fix and Perm Buffer (201067; Fluidigm). Fixed and stained cells were run for data acquisition by the CyTOF2 Mass Cytometer at the Flow Cytometry Cores at the University of Rochester Medical Center or the Indiana University Simon Cancer Center.

Mass Cytometry Data Preprocessing and Analysis

Data were obtained from 7 independent sample collections, with each experiment performed using pancreata from *Gnat3*^{-/-};KC^{ERT} accompanied by KC^{ERT} for comparison. Analysis of normalized FCS files was performed using the Premium CytoBank Software (cytobank.org). Data were assessed for staining quality, normalized by internal bead standards, and then live singlet cell events were identified by the combination of Ir191 DNA Intercalator, Event Length, and Pt195 Cisplatin staining. Filtered live single cells were exported as new FCS files for further analysis using FCS express 7 cytometry software (De Novo Software, Pasadena, CA). To avoid batch effects within the data analysis, each batch of KC^{ERT} and *Gnat3*^{-/-};KC^{ERT} pancreata were analyzed separately, and then comparisons were done using cell frequencies.

Single-Cell RNA Sequencing and Analysis

Single-cell RNA sequencing was performed in duplicate for both KC^{ERT} and *Gnat3*^{-/-};KC^{ERT} pancreata and once for the *Kras*^{G12D/+}; *Ptf1a*^{Cre/+} pancreas shown in Figure 7A–C. To obtain a single cell suspension, pancreas tissue was mechanically and chemically digested as detailed above for the mass cytometry analysis. Dead cells were excluded using MACS Dead Cell Removal Kit (130-090-101; Miltenyi Biotec Inc, Bergisch Gladbach, Germany). The 10X Genomics Platform at the University of Michigan Advanced Genomics Core

was used for single-cell cDNA library preparation and sequencing. Samples were sequenced using paired-end 50 cycle reads on HiSeq 4000 (first 2 samples) or the NovaSeq 6000 (second 2 samples) (Illumina, San Diego, CA) to a depth of 100,000 reads. Raw data were then processed, aligned, and filtered using the default setting of Cellranger version 3.0 at the University of Michigan Advanced Genomics Core. R package, Seurat version 3.0 (<http://www.satijalab.org/seurat>) was used for analysis.⁷⁵ Downstream analysis was performed as previously described.⁴¹ Briefly, data were filtered to include cells with at least 100 genes and genes identified in more than 3 cells. Data were then normalized using the `NormalizeData` function with a scale factor of 10,000 and the `LogNormalize` normalization method. Variable genes in the data set were identified using `FindVariableFeatures` function; the data were then scaled and centered using linear regression on the counts. Principal component analysis was run using `RunPCA` function on the variable genes identified. Batch correction was performed using the R package Harmony (<https://github.com/immunogenomics/harmony>).⁷⁶ `FindNeighbors` and `FindClusters` at a resolution of 1.2–2.0 were used to identify cell clusters. Cell clusters were visualized using UMAP algorithms. To define cell clusters, `FindAllMarkers` table was generated, and user-defined criteria were used for final cell population definitions. Differentially expressed gene heatmaps were manually annotated to remove B-cell and acinar contamination.

CXCL2 ELISA

Tissues were collected fresh from the head, body, and tail of the pancreas, immediately frozen in liquid nitrogen, and stored at -80°C . To acquire lysate, tissue was added to a metal bead and was homogenized in RIPA lysis buffer supplemented with protease inhibitor cocktail (PIA32965; Thermo Fisher Scientific) and PhosSTOP phosphatase inhibitor cocktail (4906845001; Millipore-Sigma) by using the TissueLyser LT (Qiagen, Hilden, Germany) for 3 minutes at 50 oscillations per second. The homogenate was collected, and samples were centrifuged at 12,700 RPM for 20 minutes at 4°C to remove debris. Supernatant was transferred into a new tube, and protein concentration was determined by BCA assay (23227; Thermo Fisher). Quantikine ELISA for CXCL2 (MM200; R&D Systems) was performed according to the manufacturer's protocol. Briefly, 120 μg of protein per well was added in duplicate to the Quantikine ELISA, using Calibrator Diluent to standardize volume to 50 μL . After washing, addition of CXCL2 detecting horseradish peroxidase conjugated secondary, washing, and then reaction solution, samples were measured at 450 nm with a wavelength correction of 540 nm. A standard curve was used to determine the concentration of CXCL2 per protein lysate, with duplicate samples levels averaged. Head, body, and tail samples from each pancreas were also averaged for the resulting CXCL2 levels per each mouse.

In Situ Hybridization

Pancreatic tissues were fixed overnight in Z-fix, embedded in paraffin, and sectioned as detailed above. In

situ hybridizations were performed with the colorimetric RNAScope 2.5 HD Reagent Kit - RED (322350; Advanced Cell Diagnostics Inc, Newark, CA) according to the manufacturer's protocol for *mCxcl2* (437581; Advanced Cell Diagnostics Inc), negative control probe *DapB* (310043; Advanced Cell Diagnostics Inc), and positive control probe *Mm-Ppib* (313911; Advanced Cell Diagnostics Inc). Briefly, paraffin-embedded sections were baked for 1 hour at 55°C before staining. Slides were then deparaffinized with HistoClear (National Diagnostics, Atlanta, GA) and treated with hydrogen peroxide for 10 minutes at room temperature. Target retrieval was performed in a steamer for 15 minutes, and then the slides were treated with the ProteasePlus (Theramedix, San Francisco, CA) solution for 15 minutes at 40°C . After this, the probe hybridized for 2 hours at 40°C , and the signal was amplified using the AMP materials provided in the RNAScope 2.5 HD Reagent Kit - RED. The signal was developed using reagent A and reagent B at 1:60 ratio. Once completed, the samples were counterstained with Mayer's hematoxylin, dried for 15 minutes at 60°C , and mounted with Cytoseal (Thermo Scientific).

Statistics

All statistics were analyzed by using GraphPad Prism 8.4.0 (San Diego, CA). Statistics for comparing 2 groups was done by unpaired Student *t* tests, except for the mass cytometry data where the Mann-Whitney test for nonparametric samples was corrected for multiple comparisons by the Benjamini-Hochberg approach.⁷⁷ For all single-cell RNA sequencing data, statistical significance was determined by using the nonparametric Wilcoxon rank sum test with Bonferroni corrected *P* values. Kaplan-Meier curve statistics were calculated by the log-rank (Mantel-Cox) test. *P* < .05 and *P* adjusted < .05 were considered statistically significant. *P* values and *P* adjusted values are listed for all, with ns = no significance.

All authors had access to the study data and have reviewed and approved the final manuscript.

References

1. American Cancer Society. Cancer facts & figures. Atlanta, GA: American Cancer Society, 2020.
2. Rahib L, Smith BD, Aizenberg R, Rosenzweig AB, Fleshman JM, Matrisian LM. Projecting cancer incidence and deaths to 2030: the unexpected burden of thyroid, liver, and pancreas cancers in the United States. *Cancer Res* 2014;74:2913–2921.
3. Werner J, Combs SE, Springfield C, Hartwig W, Hackert T, Buchler MW. Advanced-stage pancreatic cancer: therapy options. *Nat Rev Clin Oncol* 2013; 10:323–333.
4. Ansari D, Tingstedt B, Andersson B, Holmquist F, Sturesson C, Williamsson C, Sasor A, Borg D, Bauden M, Andersson R. Pancreatic cancer: yesterday, today and tomorrow. *Future Oncol* 2016;12:1929–1946.
5. Bockman DE, Boydston WR, Anderson MC. Origin of tubular complexes in human chronic pancreatitis. *Am J Surg* 1982;144:243–249.

6. Wagner M, Luhrs H, Kloppel G, Adler G, Schmid RM. Malignant transformation of duct-like cells originating from acini in transforming growth factor transgenic mice. *Gastroenterology* 1998;115:1254–1262.
7. Habbe N, Shi G, Meguid RA, Fendrich V, Esni F, Chen H, Feldmann G, Stoffers DA, Konieczny SF, Leach SD, Maitra A. Spontaneous induction of murine pancreatic intraepithelial neoplasia (mPanIN) by acinar cell targeting of oncogenic Kras in adult mice. *Proc Natl Acad Sci U S A* 2008;105:18913–18918.
8. Ardito CM, Gruner BM, Takeuchi KK, Lubeseder-Martellato C, Teichmann N, Mazur PK, Delgiorno KE, Carpenter ES, Halbrook CJ, Hall JC, Pal D, Briel T, Herner A, Trajkovic-Arsic M, Sipos B, Liou GY, Storz P, Murray NR, Threadgill DW, Sibilio M, Washington MK, Wilson CL, Schmid RM, Raines EW, Crawford HC, Siveke JT. EGF receptor is required for KRAS-induced pancreatic tumorigenesis. *Cancer Cell* 2012;22:304–317.
9. Biankin AV, Waddell N, Kassahn KS, Gingras MC, Muthuswamy LB, Johns AL, Miller DK, Wilson PJ, Patch AM, Wu J, Chang DK, Cowley MJ, Gardiner BB, Song S, Harliwong I, Idrisoglu S, Nourse C, Nourbakhsh E, Manning S, Wani S, Gongora M, Pajic M, Scarlett CJ, Gill AJ, Pinho AV, Rooman I, Anderson M, Holmes O, Leonard C, Taylor D, Wood S, Xu Q, Nones K, Fink JL, Christ A, Bruxner T, Cloonan N, Kolle G, Newell F, Pinese M, Mead RS, Humphris JL, Kaplan W, Jones MD, Colvin EK, Nagrial AM, Humphrey ES, Chou A, Chin VT, Chantrill LA, Mawson A, Samra JS, Kench JG, Lovell JA, Daly RJ, Merrett ND, Toon C, Epari K, Nguyen NQ, Barbour A, Zeps N, Kakkar N, Zhao F, Wu YQ, Wang M, Muzny DM, Fisher WE, Brunicardi FC, Hodges SE, Reid JG, Drummond J, Chang K, Han Y, Lewis LR, Dinh H, Buhay CJ, Beck T, Timms L, Sam M, Begley K, Brown A, Pai D, Panchal A, Buchner N, De Borja R, Denroche RE, Yung CK, Serra S, Onetto N, Mukhopadhyay D, Tsao MS, Shaw PA, Petersen GM, Gallinger S, Hruban RH, Maitra A, Iacobuzio-Donahue CA, Schulick RD, Wolfgang CL, Morgan RA, Lawlor RT, Capelli P, Corbo V, Scardoni M, Tortora G, Tempero MA, Mann KM, Jenkins NA, Perez-Mancera PA, Adams DJ, Largaespada DA, Wessels LF, Rust AG, Stein LD, Tuveson DA, Copeland NG, Musgrove EA, Scarpa A, Eshleman JR, Hudson TJ, Sutherland RL, Wheeler DA, Pearson JV, McPherson JD, Gibbs RA, Grimmond SM. Pancreatic cancer genomes reveal aberrations in axon guidance pathway genes. *Nature* 2012;491:399–405.
10. Jones S, Zhang X, Parsons DW, Lin JC, Leary RJ, Angenendt P, Mankoo P, Carter H, Kamiyama H, Jimeno A, Hong SM, Fu B, Lin MT, Calhoun ES, Kamiyama M, Walter K, Nikolskaya T, Nikolsky Y, Hartigan J, Smith DR, Hidalgo M, Leach SD, Klein AP, Jaffee EM, Goggins M, Maitra A, Iacobuzio-Donahue C, Eshleman JR, Kern SE, Hruban RH, Karchin R, Papadopoulos N, Parmigiani G, Vogelstein B, Velculescu VE, Kinzler KW. Core signaling pathways in human pancreatic cancers revealed by global genomic analyses. *Science* 2008;321:1801–1806.
11. Collisson EA, Bailey P, Chang DK, Biankin AV. Molecular subtypes of pancreatic cancer. *Nat Rev Gastroenterol Hepatol* 2019;16:207–220.
12. Ryan DP, Hong TS, Bardeesy N. Pancreatic adenocarcinoma. *N Engl J Med* 2014;371:2140–2141.
13. Inman KS, Francis AA, Murray NR. Complex role for the immune system in initiation and progression of pancreatic cancer. *World J Gastroenterol* 2014;20:11160–11181.
14. Looi C-K, Chung FF-L, Leong C-O, Wong S-F, Rosli R, Mai C-W. Therapeutic challenges and current immunomodulatory strategies in targeting the immunosuppressive pancreatic tumor microenvironment. *J Exp Clin Cancer Res* 2019;38:162.
15. Clark CE, Hingorani SR, Mick R, Combs C, Tuveson DA, Vonderheide RH. Dynamics of the immune reaction to pancreatic cancer from inception to invasion. *Cancer Res* 2007;67:9518–9527.
16. Hosein AN, Huang H, Wang Z, Parmar K, Du W, Huang J, Maitra A, Olson E, Verma U, Brekken RA. Cellular heterogeneity during mouse pancreatic ductal adenocarcinoma progression at single-cell resolution. *JCI Insight* 2019;25:2194–2205.
17. Li J, Byrne KT, Yan F, Yamazoe T, Chen Z, Baslan T, Richman LP, Lin JH, Sun YH, Rech AJ, Balli D, Hay CA, Sela Y, Merrell AJ, Liudahl SM, Gordon N, Norgard RJ, Yuan S, Yu S, Chao T, Ye S, Eisinger-Mathason TSK, Faryabi RB, Tobias JW, Lowe SW, Coussens LM, Wherry EJ, Vonderheide RH, Stanger BZ. Tumor cell-intrinsic factors underlie heterogeneity of immune cell infiltration and response to immunotherapy. *Immunity* 2018;49:178–193.e7.
18. Sinha S, Fu YY, Grimont A, Ketcham M, Lafaro K, Saglimbeni JA, Askan G, Bailey JM, Melchor JP, Zhong Y, Joo MG, Grbovic-Huezo O, Yang IH, Basturk O, Baker L, Park Y, Kurtz RC, Tuveson D, Leach SD, Pasricha PJ. PanIN neuroendocrine cells promote tumorigenesis via neuronal cross-talk. *Cancer Res* 2017;77:1868–1879.
19. Delgiorno KE, Hall JC, Takeuchi KK, Pan FC, Halbrook CJ, Washington MK, Olive KP, Spence JR, Sipos B, Wright CV, Wells JM, Crawford HC. Identification and manipulation of biliary metaplasia in pancreatic tumors. *Gastroenterology* 2014;146:233–244.e5.
20. O’Leary CE, Schneider C, Locksley RM. Tuft cells: systemically dispersed sensory epithelia integrating immune and neural circuitry. *Annu Rev Immunol* 2019;37:47–72.
21. Saunders CJ, Christensen M, Finger TE, Tizzano M. Cholinergic neurotransmission links solitary chemosensory cells to nasal inflammation. *Proc Natl Acad Sci U S A* 2014;111:6075–6080.
22. Howitt MR, Lavoie S, Michaud M, Blum AM, Tran SV, Weinstock JV, Gallini CA, Redding K, Margolskee RF, Osborne LC, Artis D, Garrett WS. Tuft cells, taste-chemosensory cells, orchestrate parasite type 2 immunity in the gut. *Science* 2016;351:1329–1333.
23. von Moltke J, Ji M, Liang HE, Locksley RM. Tuft-cell-derived IL-25 regulates an intestinal ILC2-epithelial response circuit. *Nature* 2016;529:221–225.

24. Ting HA, von Moltke J. The immune function of tuft cells at gut mucosal surfaces and beyond. *J Immunol* 2019; 202:1321–1329.
25. Roper SD, Chaudhari N. Taste buds: cells, signals and synapses. *Nat Rev Neurosci* 2017;18:485–497.
26. Steele CW, Karim SA, Leach JDG, Bailey P, Upstill-Goddard R, Rishi L, Foth M, Bryson S, McDaid K, Wilson Z, Eberlein C, Candido JB, Clarke M, Nixon C, Connelly J, Jamieson N, Carter CR, Balkwill F, Chang DK, Evans TRJ, Strathdee D, Biankin AV, Nibbs RJB, Bary ST, Sansom OJ, Morton JP. CXCR2 inhibition profoundly suppresses metastases and augments immunotherapy in pancreatic ductal adenocarcinoma. *Cancer Cell* 2016;29:832–845.
27. Chao T, Furth EE, Vonderheide RH. CXCR2-dependent accumulation of tumor-associated neutrophils regulates T-cell immunity in pancreatic ductal adenocarcinoma. *Cancer Immunol Res* 2016;4:968–982.
28. Glendinning JI, Bloom LD, Onishi M, Zheng KH, Damak S, Margolskee RF, Spector AC. Contribution of alpha-gustducin to taste-guided licking responses of mice. *Chem Senses* 2005;30:299–316.
29. Wong GT, Gannon KS, Margolskee RF. Transduction of bitter and sweet taste by gustducin. *Nature* 1996; 381:796–800.
30. Wu CY, Carpenter ES, Takeuchi KK, Halbrook CJ, Peverley LV, Bien H, Hall JC, DelGiorno KE, Pal D, Song Y, Shi C, Lin RZ, Crawford HC. PI3K regulation of RAC1 is required for KRAS-induced pancreatic tumorigenesis in mice. *Gastroenterology* 2014;147:1405–1416. e7.
31. Huang L, Holtzinger A, Jagan I, BeGora M, Lohse I, Ngai N, Nostro C, Wang R, Muthuswamy LB, Crawford HC, Arrowsmith C, Kalloger SE, Renouf DJ, Connor AA, Cleary S, Schaeffer DF, Roehrl M, Tsao MS, Gallinger S, Keller G, Muthuswamy SK. Ductal pancreatic cancer modeling and drug screening using human pluripotent stem cell- and patient-derived tumor organoids. *Nat Med* 2015;21:1364–1371.
32. Yokoyama M, Ebert M, Funatomi H, Friess H, Buchler M, Johnson G, Korc M. Amphiregulin is a potent mitogen in human pancreatic-cancer cells: correlation with patient survival. *Int J Oncol* 1995;6:625–631.
33. Ebert M, Yokoyama M, Kobrin MS, Friess H, Lopez ME, Buchler MW, Johnson GR, Korc M. Induction and expression of amphiregulin in human pancreatic cancer. *Cancer Res* 1994;54:3959–3962.
34. Chen HT, Zheng JM, Zhang YZ, Yang M, Wang YL, Man XH, Chen Y, Cai QC, Li ZS. Overexpression of YKL-40 predicts poor prognosis in patients undergoing curative resection of pancreatic cancer. *Pancreas* 2017; 46:323–334.
35. Ijichi H, Chytil A, Gorska AE, Aakre ME, Bieri B, Tada M, Mohri D, Miyabayashi K, Asaoka Y, Maeda S, Ikenoue T, Tateishi K, Wright CV, Koike K, Omata M, Moses HL. Inhibiting Cxcr2 disrupts tumor-stromal interactions and improves survival in a mouse model of pancreatic ductal adenocarcinoma. *J Clin Invest* 2011; 121:4106–4117.
36. Wenthe MN, Gaida MM, Mayer C, Michalski CW, Haag N, Giese T, Felix K, Bergmann F, Giese NA, Friess H. Expression and potential function of the CXC chemokine CXCL16 in pancreatic ductal adenocarcinoma. *Int J Oncol* 2008;33:297–308.
37. Roy I, Boyle KA, Vonderhaar EP, Zimmerman NP, Gorse E, Mackinnon AC, Hwang RF, Franco-Barraza J, Cukierman E, Tsai S, Evans DB, Dwinell MB. Cancer cell chemokines direct chemotaxis of activated stellate cells in pancreatic ductal adenocarcinoma. *Lab Invest* 2017; 97:302–317.
38. Shi W, Qiu W, Wang W, Zhou X, Zhong X, Tian G, Deng A. Osteoprotegerin is up-regulated in pancreatic cancers and correlates with cancer-associated new-onset diabetes. *Biosci Trends* 2014;8:322–326.
39. Pan FC, Bankaitis ED, Boyer D, Xu X, Van de Castele M, Magnuson MA, Heimberg H, Wright CV. Spatiotemporal patterns of multipotentiality in Ptf1a-expressing cells during pancreas organogenesis and injury-induced facultative restoration. *Development* 2013;140:751–764.
40. Karamitopoulou E. Tumour microenvironment of pancreatic cancer: immune landscape is dictated by molecular and histopathological features. *Br J Cancer* 2019;121:5–14.
41. Zhang Y, Lazarus J, Steele NG, Yan W, Lee HJ, Nwosu ZC, Halbrook CJ, Menjivar RE, Kemp SB, Sirihorachai VR, Velez-Delgado A, Donahue K, Carpenter ES, Brown KL, Irizarry-Negron V, Nevison AC, Vinta A, Anderson MA, Crawford HC, Lyssiotis CA, Frankel TL, Bednar F, Pasca di Magliano M. Regulatory T-cell depletion alters the tumor microenvironment and accelerates pancreatic carcinogenesis. *Cancer Discov* 2020;10:422–439.
42. Dragomir A-CD, Sun R, Choi H, Laskin JD, Laskin DL. Role of galectin-3 in classical and alternative macrophage activation in the liver following acetaminophen intoxication. *J Immunol* 2012;189:5934–5941.
43. Guo Y, Lin C, Xu P, Wu S, Fu X, Xia W, Yao M. AGEs induced autophagy impairs cutaneous wound healing via stimulating macrophage polarization to M1 in diabetes. *Scientific Reports* 2016;6:36416.
44. Miller CN, Proekt I, von Moltke J, Wells KL, Rajpurkar AR, Wang H, Rattay K, Khan IS, Metzger TC, Pollack JL, Fries AC, Lwin WW, Wigton EJ, Parent AV, Kyewski B, Erle DJ, Hogquist KA, Steinmetz LM, Locksley RM, Anderson MS. Thymic tuft cells promote an IL-4-enriched medulla and shape thymocyte development. *Nature* 2018;559:627–631.
45. Damuzzo V, Pinton L, Desantis G, Solito S, Marigo I, Bronte V, Mandruzzato S. Complexity and challenges in defining myeloid-derived suppressor cells. *Cytometry B Clin Cytom* 2015;88:77–91.
46. Ouzounova M, Lee E, Piranlioglu R, El Andaloussi A, Kolhe R, Demirci MF, Marasco D, Asm I, Chadli A, Hassan KA, Thangaraju M, Zhou G, Arbab AS, Cowell JK, Korkaya H. Monocytic and granulocytic myeloid derived suppressor cells differentially regulate spatiotemporal tumour plasticity during metastatic cascade. *Nat Commun* 2017;8:14979.

47. Thyagarajan A, Alshehri MSA, Miller KLR, Sherwin CM, Travers JB, Sahu RP. Myeloid-derived suppressor cells and pancreatic cancer: implications in novel therapeutic approaches. *Cancers (Basel)* 2019;11.
48. Becht E, McInnes L, Healy J, Dutertre C-A, Kwok IWH, Ng LG, Ginhoux F, Newell EW. Dimensionality reduction for visualizing single-cell data using UMAP. *Nature Biotechnology* 2019;37:38–44.
49. Ohlund D, Handy-Santana A, Biffi G, Elyada E, Almeida AS, Ponz-Sarvisé M, Corbo V, Oni TE, Hearn SA, Lee EJ, Chio I, Hwang CI, Tiriach H, Baker LA, Engle DD, Feig C, Kultti A, Egeblad M, Fearon DT, Crawford JM, Clevers H, Park Y, Tuveson DA. Distinct populations of inflammatory fibroblasts and myofibroblasts in pancreatic cancer. *J Exp Med* 2017; 214:579–596.
50. Lehrer RI, Ganz T. Cathelicidins: a family of endogenous antimicrobial peptides. *Curr Opin Hematol* 2002;9:18–22.
51. Kruzel ML, Zimecki M, Actor JK. Lactoferrin in a context of inflammation-induced pathology. *Front Immunol* 2017; 8:1438.
52. Park SY, Jing X, Gupta D, Dziarski R. Peptidoglycan recognition protein 1 enhances experimental asthma by promoting Th2 and Th17 and limiting regulatory T cell and plasmacytoid dendritic cell responses. *J Immunol* 2013;190:3480–3492.
53. Ibrahim HR, Matsuzaki T, Aoki T. Genetic evidence that antibacterial activity of lysozyme is independent of its catalytic function. *FEBS Lett* 2001;506:27–32.
54. Bent R, Moll L, Grabbe S, Bros M. Interleukin-1 beta: a friend or foe in malignancies? *Int J Mol Sci* 2018;19.
55. Cui X, Liu Y, Wan C, Lu C, Cai J, He S, Ni T, Zhu J, Wei L, Zhang Y, Qian H. Decreased expression of SERPINB1 correlates with tumor invasion and poor prognosis in hepatocellular carcinoma. *J Mol Histol* 2014;45:59–68.
56. Purvis GSD, Solito E, Thiernemann C. Annexin-A1: therapeutic potential in microvascular disease. *Front Immunol* 2019;10:938.
57. Rosenbaum S, Kreft S, Etich J, Frie C, Stermann J, Grskovic I, Frey B, Mielenz D, Poschl E, Gajpl U, Paulsson M, Brachvogel B. Identification of novel binding partners (annexins) for the cell death signal phosphatidylserine and definition of their recognition motif. *J Biol Chem* 2011;286:5708–5716.
58. Acharyya S, Oskarsson T, Vanharanta S, Malladi S, Kim J, Morris PG, Manova-Todorova K, Leversha M, Hogg N, Seshan VE, Norton L, Brogi E, Massague J. A CXCL1 paracrine network links cancer chemoresistance and metastasis. *Cell* 2012;150:165–178.
59. Jaffer T, Ma D. The emerging role of chemokine receptor CXCR2 in cancer progression. *Translational Cancer Research* 2016;5(Suppl 4):S616–S628.
60. Wollny D, Zhao S, Everlien I, Lun X, Brunken J, Brüne D, Ziebell F, Tabansky I, Weichert W, Marciniak-Czochra A, Martin-Villalba A. Single-cell analysis uncovers clonal acinar cell heterogeneity in the adult pancreas. *Dev Cell* 2016;39:289–301.
61. Hingorani SR, Petricoin EF, Maitra A, Rajapakse V, King C, Jacobetz MA, Ross S, Conrads TP, Veenstra TD, Hitt BA, Kawaguchi Y, Johann D, Liotta LA, Crawford HC, Putt ME, Jacks T, Wright CV, Hruban RH, Lowy AM, Tuveson DA. Preinvasive and invasive ductal pancreatic cancer and its early detection in the mouse. *Cancer Cell* 2003;4:437–450.
62. Bailey JM, Alsina J, Rasheed ZA, McAllister FM, Fu YY, Plentz R, Zhang H, Pasricha PJ, Bardeesy N, Matsui W, Maitra A, Leach SD. DCLK1 marks a morphologically distinct subpopulation of cells with stem cell properties in preinvasive pancreatic cancer. *Gastroenterology* 2014; 146:245–256.
63. Westphalen CB, Asfaha S, Hayakawa Y, Takemoto Y, Lukin DJ, Nuber AH, Brandtner A, Setlik W, Remotti H, Muley A, Chen X, May R, Houchen CW, Fox JG, Gershon MD, Quante M, Wang TC. Long-lived intestinal tuft cells serve as colon cancer-initiating cells. *J Clin Invest* 2014;124:1283–1295.
64. Chandrakesan P, Yao J, Qu D, May R, Weygant N, Ge Y, Ali N, Sureban SM, Gude M, Vega K, Bannerman-Menson E, Xia L, Bronze M, An G, Houchen CW. Dclk1, a tumor stem cell marker, regulates pro-survival signaling and self-renewal of intestinal tumor cells. *Molecular Cancer* 2017;16:30.
65. Youn JI, Collazo M, Shalova IN, Biswas SK, Gabrilovich DI. Characterization of the nature of granulocytic myeloid-derived suppressor cells in tumor-bearing mice. *J Leukoc Biol* 2012;91:167–181.
66. Zhang Y, Velez-Delgado A, Mathew E, Li D, Mendez FM, Flannagan K, Rhim AD, Simeone DM, Beatty GL, Pasca di Magliano M. Myeloid cells are required for PD-1/PD-L1 checkpoint activation and the establishment of an immunosuppressive environment in pancreatic cancer. *Gut* 2017;66:124–136.
67. Gulbransen BD, Clapp TR, Finger TE, Kinnamon SC. Nasal solitary chemoreceptor cell responses to bitter and trigeminal stimulants in vitro. *J Neurophysiol* 2008; 99:2929–2937.
68. DelGiorno KE, Chung CY, Vavinskaya V, Maurer HC, Novak SW, Lytle NK, Ma Z, Girardi RR, Wang D, Fang L, Naeem RF, Andrade LR, Ali WH, Tseng H, Tsui C, Gubbala VB, Ridinger-Saison M, Ohmoto M, Erikson GA, O'Connor C, Shokhirev MN, Hah N, Urade Y, Matsumoto I, Kaech SM, Singh PK, Manor U, Olive KP, Wahl GM. Tuft cells inhibit pancreatic tumorigenesis in mice by producing prostaglandin D2. *Gastroenterology* 2020.
69. Roy N, Hebrok M. Regulation of cellular identity in cancer. *Dev Cell* 2015;35:674–684.
70. Zhang Y, Morris JPt, Yan W, Schofield HK, Gurney A, Simeone DM, Millar SE, Hoey T, Hebrok M, Pasca di Magliano M. Canonical wnt signaling is required for pancreatic carcinogenesis. *Cancer Res* 2013; 73:4909–4922.
71. Wen HJ, Gao S, Wang Y, Ray M, Magnuson MA, Wright CVE, Di Magliano MP, Frankel TL, Crawford HC. Myeloid cell-derived HB-EGF drives tissue recovery after pancreatitis. *Cell Mol Gastroenterol Hepatol* 2019; 8:173–192.
72. Roy N, Takeuchi KK, Ruggeri JM, Bailey P, Chang D, Li J, Leonhardt L, Puri S, Hoffman MT, Gao S, Halbrook CJ, Song Y, Ljungman M, Malik S, Wright CV,

- Dawson DW, Biankin AV, Hebrok M, Crawford HC. PDX1 dynamically regulates pancreatic ductal adenocarcinoma initiation and maintenance. *Genes Dev* 2016; 30:2669–2683.
73. Shamir ER, Pappalardo E, Jorgens DM, Coutinho K, Tsai WT, Aziz K, Auer M, Tran PT, Bader JS, Ewald AJ. Twist1-induced dissemination preserves epithelial identity and requires E-cadherin. *J Cell Biol* 2014; 204:839–856.
 74. Bertaux-Skeirik N, Wunderlich M, Teal E, Chakrabarti J, Biesiada J, Mahe M, Sundaram N, Gabre J, Hawkins J, Jian G, Engevik AC, Yang L, Wang J, Goldenring JR, Qualls JE, Medvedovic M, Helmrath MA, Diwan T, Mulloy JC, Zavros Y. CD44 variant isoform 9 emerges in response to injury and contributes to the regeneration of the gastric epithelium. *J Pathol* 2017;242:463–475.
 75. Butler A, Hoffman P, Smibert P, Papalexi E, Satija R. Integrating single-cell transcriptomic data across different conditions, technologies, and species. *Nat Biotechnol* 2018;36:411–420.
 76. Korsunsky I, Millard N, Fan J, Slowikowski K, Zhang F, Wei K, Baglaenko Y, Brenner M, Loh PR, Raychaudhuri S. Fast, sensitive and accurate integration of single-cell data with Harmony. *Nat Methods* 2019; 16:1289–1296.
 77. Benjamini Y, Hochberg Y. Controlling the false discovery rate: a practical and powerful approach to multiple testing. *J Roy Stat Soc Series B* 1995;57:289–300.

Received April 8, 2020. Accepted August 26, 2020.

Correspondence

Address correspondence to: Howard Crawford, PhD, 1500 East Medical Center Drive, Ann Arbor, Michigan 48109-5936. e-mail: howcraw@umich.edu; fax: (734) 936-8813.

Acknowledgments

The authors thank Drs Kathleen Delgiorno and Geoffrey Wahl for helpful discussions and feedback on the manuscript. They thank Dr Senthil Muthuswamy for supplements for the PTOM organoid media and Elizabeth Field for proofreading. They thank the members of the Pancreatic Cancer Research Initiative at the University of Michigan for helpful discussions.

CRedit Authorship Contributions

Howard Crawford, PhD (Conceptualization: Lead; Funding acquisition: Lead; Investigation: Supporting; Methodology: Equal; Project administration: Lead; Supervision: Lead; Writing – original draft: Equal; Writing – review & editing: Equal)

Megan T. Hoffman (Data curation: Lead; Formal analysis: Lead; Investigation: Lead; Methodology: Equal; Writing – original draft: Equal; Writing – review & editing: Equal)

Samantha B. Kemp (Formal analysis: Supporting; Methodology: Supporting)

Daniel J. Salas-Escabillas (Data curation: Supporting; Investigation: Supporting)

Yaqing Zhang (Formal analysis: Supporting)

Nina G. Steele (Formal analysis: Supporting)

Stephanie The (Formal analysis: Supporting; Methodology: Supporting)

Daniel Long (Data curation: Supporting; Methodology: Supporting)

Simone Benitz (Investigation: Supporting)

Wei Yan (Formal analysis: Supporting)

Filip Bednar (Formal analysis: Supporting)

Robert F. Margolskee (Resources: Supporting)

Marina Pasca di Magliano (Conceptualization: Supporting; Methodology: Supporting)

Hui-Ju Wen (Methodology: Supporting; Supervision: Supporting)

Conflicts of interest

The authors disclose no conflicts.

Funding

Supported by the NIH/NCI grant R01CA247516 to HCC and Cancer Moonshot Initiative (U01CA224145) to HCC and MPdM. This project was also supported by NIH/ NCI grants R01CA151588, R01CA198074, the University of Michigan Cancer Center Support Grant (NCI P30CA046592), the American Cancer Society to MPdM, and NCI-R50CA232985 to YZ. This project was also supported by 3P30CA04659228S2 (Administrative Supplement to the Cancer Center Core Grant) to HCC and MPdM. MTH was supported by the Rogel Graduate Fellowship and SBK by the Marantette Graduate Fellowship. FB was funded by the Association for Academic Surgery Joel Roslyn Award. NS is a recipient of the American Cancer Society Postdoctoral Award. SBK was supported by T32GM113900; NS was supported by T32CA009676. ST and AR were supported through CCSG P30 CA046592, Institutional Research Grants from the University of Michigan, NCI R37CA214955-01A1, and a Research Scholar Grant from the American Cancer Society (RSG-16-005-01).